Available online at www.sciencedirect.com

ScienceDirect

Advances in Space Research 77 (2026) 9174–9200

ADVANCES IN SPACE RESEARCH (a COSPAR publication)

www.elsevier.com/locate/asr

Advanced techniques for the stochastic fragmentation event characterization from a single fragment orbital state

Paola Grattagliano *, Marco Felice Montaruli, Pierluigi Di Lizia

Politecnico di Milano, Department of Aerospace Science and Technology (DAER), Via G. La Masa 34, Milan 20156, Italy

Received 6 May 2025; received in revised form 6 October 2025; accepted 14 February 2026
Available online 24 February 2026

Abstract

The growing population of objects in low Earth orbits poses increasing risks to satellites. Fragmentation events—collisions, explosions, and material degradation—are the main contributors to orbital overcrowding, generating further debris.

This research develops a tool for characterizing fragmentation events, with emphasis on determining their epochs. Knowing the epoch improves observation planning and debris prediction. This tool also achieves fragment–event association and the rejection of unrelated objects. This enhances the cataloguing of newly generated debris.

The method models the event as a collision between the parent body and a fragment, computing collision probabilities over time. The highest probability indicates potential fragmentation epochs, from which a single estimate is derived. Gaussian mixtures are used to represent and propagate uncertainty, offering more accurate probability computations by capturing non-linearities that Gaussian assumptions could not.

Validation through numerical analysis shows that, while perturbations and orbit determination errors degrade accuracy, the correct epoch is always among the candidates. Real data tests confirm the method robustness in operational scenarios. The algorithm proves reliable and requires only one fragment state and the parent ephemeris, making it highly practical.

Keywords: Fragmentations; Space surveillance and tracking; Space traffic management; Conjunction analysis; Gaussian mixtures

1. Introduction

The proliferation of Resident Space Objects (RSO) in Low Earth Orbit (LEO) has emerged as a matter of significant concern, particularly in the context of the advancement of space services. The most recent data about to the quantity of non-functional orbiting objects has been provided by the ESA Space Debris Office. The data indicates that approximately 19,590 satellites have been placed into Earth orbit in more than 60 years of activities, resulting in the current presence of 54,000 space objects with dimensions over approximately 10 cm, 1.2 million debris with dimensions between 1 cm and 10 cm and 1.4 billion debris with smaller dimensions (ESA, 2024b). In this context, these debris may be defined as *all human made objects including fragments and elements thereof, in Earth orbit or re-entering the atmosphere, that are non-functional* (IADC, 2021). This population poses a significant threat to both future and current missions, as the impact of a debris with a functioning satellite has the potential to end its operational life or cause damage to parts of it. Conversely, the presence of space debris can generate additional fragments, which may in turn trigger a chain reaction. This phenomenon was studied by Donald Kessler, who hypothesized that the excessive accumulation of space debris

* Corresponding author.
E-mail addresses: paola.grattagliano@polimi.it (P. Grattagliano), marcofelice.montaruli@polimi.it (M.F. Montaruli), pierluigi.dilizia@polimi.it (P. Di Lizia).

https://doi.org/10.1016/j.asr.2026.02.060
0273-1177/

could initiate a cascading sequence of collisions and explosions. Such a process would result in an exponential increase in the number of artificial objects in orbit, thereby rendering spaceflight exceedingly hazardous (Kessler and Cour-Palais, 1978). Although we have not yet reached the scenario predicted by Kessler, fragmentation events are currently the dominant source of space debris (ESA, 2024a).

In this framework, various initiatives are undertaken to address the challenges mentioned above. These efforts focus on tracking and cataloguing RSOs orbits, monitoring fragmentation events, and implementing countermeasures to mitigate the associated risks. At the European level, there are two significant Space Surveillance and Tracking (SST) capabilities: the SST segment of the ESA SSA program, managed through the ESA Space Debris Office, and the EUSST Consortium. The latter organizes its operations around three primary functions: sensor, processing, and service. The sensor function comprises a network of ground-based sensors dedicated to surveying and tracking space objects, which may be optical telescopes (Pastor et al., 2022; Maruskin et al., 2009), radars (Bianchi et al., 2023; Montaruli et al. (2024d); Montaruli et al. (2024b); Montaruli et al. (2024a)) or lasers (Cordelli et al., 2020). The processing function involves the analysis of SST data at a national level to produce SST information and services (Montaruli et al., 2024e). The service function provides SST services to the European user community (EUSST, 2023a). Within the service function, the Collision Avoidance service assesses collision risks and generates alerts to prevent collisions (Bonaccorsi et al., 2024). The Re-entry Analysis service evaluates the risk of uncontrolled re-entries of man-made space objects into the Earth's atmosphere and disseminates relevant information (Pardini and Anselmo, 2008; Montaruli et al., 2025). The Fragmentation Analysis service is responsible for detecting and characterizing in-orbit fragmentations, break-ups, and collisions, and for analyzing all available information regarding the involved objects (Mains et al., 2024; EUSST, 2023b).

In the context of the aforementioned background, the timely monitoring of on-orbit break-ups is of paramount importance. The immediate prediction of the trajectories of resulting fragments through models capable of forecasting the debris cloud evolution (Giudici et al. (2024); Letizia et al. (2015); Matney et al. (1999); Matney (2000)) is necessary to assess the likelihood of subsequent collisions, which may in turn give rise to additional fragments. Furthermore, early fragmentations characterization activities allow for the planning of appropriate further observations aimed at preventing potential future collisions. In order to achieve these objectives, it is first necessary to detect the epoch and the location of the fragments generation from the primary object to be used as initial conditions for the aforementioned activities. This data indeed is crucial not only for predicting the cloud dispersion, but also to associate the observed fragments with a parent object.

Fragmentation events include generally explosions and collisions. Multiple methods for the detection of the epoch and the location of a fragmentation event are proposed in the current state of the art. In (Andrişan et al., 2016) the event epoch is identified through a backward propagation of each fragment of the analysed cloud. At each time step the distance between the propagated state and the centre of mass of the cloud is computed, and the event is detected where this distance reaches a minimum. In (Dimare et al., 2019) the break-up time is identified within an approach to correlate known fragments with possible parent objects. To achieve this, five distance metrics are applied (D-Criterias, Minimum Orbital Intersection Distance (MOID) and nodal distance) and investigated in terms of accuracy of the produced results. In (Slatton and McKissock, 2017) the epoch detection is achieved by applying a conjunction assessment software, after having correlated the debris to the event, and by looking for the time of convergence of the miss distance. Despite the ease and effectiveness of this method, numerous ephemerides of various fragments are assumed to be known and associable with an already catalogued parent object. The assumption of availability of many Two-Line Elements (TLEs) is leveraged in (Muciaccia et al., 2024) as well, where the PUZZLE tool is described. This tool is devoted to the break-up event detection and fragmentation epoch estimation, both in the short and long-term scenarios, through a first pruning and filtering of non-relevant TLEs, and a subsequent analysis of the orbital elements of the remaining ones. Indeed, in the vicinity of the break-up event, the generated fragments exhibit similarities in certain Keplerian elements. The knowledge of numerous precise orbital states of the fragments is necessary for the epoch estimation process; however, this represents a less frequently applicable assumption in a realistic operational scenario. In such situations, the fragmentation epoch is required shortly after the event is detected, when a small number of debris ephemerides (or a single one) is known, to plan as soon as possible further observations of the generated fragments and perform a refinement of their determined orbital states. This process improves the epoch estimation accuracy, creating a "virtuous cycle". In this context, the FRagmentation Epoch Detector (FRED) algorithm (Montaruli et al., 2023b), aims to detect the epoch of a fragmentation event, exploiting the availability of one ephemeris of the parent object and a single orbital state of a generated fragment. The approach is stochastic, and different distance metrics are investigated to identify and rank fragmentation epoch candidates by comparing the statistical distributions of MOID and relative distance between parent and fragment. The best fragmentation epoch is finally returned in terms of mean value and standard deviation.

However, FRED algorithm is subject to certain limitations, which underscore the necessity for its enhancement and, consequently, serve as a motivation for the present research. Primarily, it is necessary to address the lack of

a procedure for associating fragments with their parent objects. In fact, within FRED, this association is assumed a priori. Furthermore, FRED is characterized by a significant computational cost: as it relies on a Monte Carlo analysis, the computational expense is directly proportional to the number of samples considered. Finally, only the state of the fragment is represented stochastically, while the state of the parent object is assumed to be deterministic. This represents a simplification of the problem.

The objective of the present work is to overcome the limitations of FRED method, as previously described. In order to achieve this, the proposed approach leverages the probability of collision (inherited from Conjunction Analysis (CA) techniques) and an advanced tool for uncertainty representation, namely Gaussian mixtures. The latter choice is motivated by the need to mitigate the computational costs. The implementation of these enhancements is set to result in a novel version of FRED, referred to in this work as FRED 2.0. The work conducted to achieve these improvements is described in the following sections. In particular, Section 2 provides a step-by-step and detailed description of the tool implementation. It includes the definition of the required inputs and it outlines codes used for estimating the fragmentation epoch and associating the fragment with the parent object. In Section 3, the results of numerical simulations conducted on a fragmentation test case are discussed. The algorithm is then applied on a real break-up to test its performance in an operational scenario, as reported in Section 4. Conclusions and potential future developments of this work are finally depicted in Section 5.

2. Methodology

Let's examine the fragmentation of a space object denoted as parent, for which the most recent available ephemeris $\boldsymbol{x}^p$ is recorded at t_{eph}, to which a covariance matrix is associated, through either an Orbit Determination (OD) process or through the TLE based approach presented in Section 2.2. The fragmentation event occurs at t_0 with $t_0 > t_{eph}$, and an alert regarding the event is issued at t_a with $t_a > t_0$. Subsequently, a fragment is detected by a ground-based sensor at $t_{od} > t_a$, and the fragment orbital state $\boldsymbol{x}^f$ and covariance $\boldsymbol{P}^f$ are initially determined, being directly derived from the Initial Orbit Determination (IOD) process.

If the orbit determination were highly accurate and the physical parameters and dynamical model sufficiently realistic, it would theoretically be possible to propagate the trajectories of both parent and fragment objects in the time window from t_{eph} to t_a and to look for the epoch of minimum relative distance. However, in operational applications, the accuracy of measurements and the IOD process introduce errors in reconstructing the observed fragment state vector, making this method unreliable. As an example, Fig. 1 from (Montaruli et al., 2023c) illustrates the

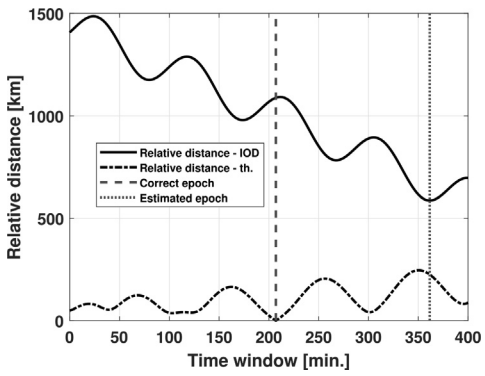

Fig. 1. Relative distance between the parent object and the mean state of one observed fragment. The dashed curve in the bottom shows the theoretical trend and the dashed straight line corresponds to the epoch of minimum value, that is the fragmentation epoch. The continuous black line shows the relative distance trend when an IOD error is introduced on the fragment mean state, and the dashed dense line corresponds to the minimum value, that is the estimated fragmentation epoch. It is possible to see that the estimated fragmentation epoch is completely different from the correct value. Source: (Montaruli et al., 2023c).

trend of relative distance over an analysis time window between the last available ephemeris of the parent object and the mean state of an observed fragment.

It can be observed that the epoch corresponding to the minimum relative distance between the fragment and parent mean states (dashed dense line on the right) differs significantly from the correct fragmentation epoch (dashed line on the left), which corresponds to the theoretical minimum relative distance (dashed black line) (Montaruli et al., 2023c). Additionally, errors arise from the mismatch between the actual fragment trajectory and the propagation model used, due to unknown actual physical parameters of the observed fragment and due to perturbation which may be simplified or even not considered. For these reasons, determining the fragmentation epoch by simply searching for the minimum relative distance between the orbital states $\boldsymbol{x}^p$ and $\boldsymbol{x}^f$, treated as deterministic variables, in the time window t_{eph} to t_a is an unreliable methodology.

The considerations above imply that OD uncertainty cannot be neglected. This motivated the choice to conduct a stochastic approach for the fragmentation epoch identification, which leaded to develop FRED algorithm (Montaruli et al., 2023c). As mentioned above, the present work shows the advancement of such algorithm, addressed as FRED 2.0, which exploits Gaussian Mixture Models (GMMs) to represent and propagate the uncertainties, differently from the Monte Carlo (MC) approach used in the original version of FRED. Another innovation of the new approach is the uncertainty association to both fragment and parent orbital states.

Section 2.1 describes the proposed algorithm, detailing both the uncertainty representation and propagation, the fragmentation epoch identification and the fragment association to the event. Then, Section 2.2 illustrates an operational procedure which can be exploited to associate a

covariance to a parent object starting from a set of TLEs, which are deterministic information.

2.1. FRED 2.0

FRED 2.0 tool is presented in this section. The algorithm takes as input the parent and a single fragment orbital state, both stochastically described in terms of mean state and covariance. First, the algorithm manages the uncertainty of both the orbital states through the GMM representation, as described in Section 2.1.1. Then, it is used both to estimate the epoch of the fragmentation event, as explained in Section 2.1.2, and to verify the association of the fragment object to the parent, through the methodology proposed in Section 2.1.3. The general flow chart of FRED 2.0 capabilities is represented in Fig. 2.

The ephemeris of the original (parent) object involved in the fragmentation is referred to as $\boldsymbol{x}^p$ and is dated to t_{eph}, epoch of the last orbital state available before the event. The covariance matrix of the parent $\boldsymbol{P}^p$ is also dated to t_{eph}, and associated to $\boldsymbol{x}^p$. This matrix could derive either from an OD process, or according to the procedure described in Section 2.2, if the ephemerides are available in the form of TLEs from a catalogue.

2.1.1. GMMs generation

According to the theory underlying GMM, any initial Gaussian distribution can be discretized into a series of smaller Gaussians (Vittaldev, 2015). This implies that a certain Probability Density Function (PDF) can be approximated through a weighted sum of N Gaussian PDFs with smaller covariances, as reported in Eq. 1:

$$p(\boldsymbol{x}) \approx \sum_{i=1}^{N} \alpha_i p_g(\boldsymbol{x}; \boldsymbol{\mu}_i, \boldsymbol{P}_i) \sum_{i=1}^{N} \alpha_i = 1 \tag{1}$$

The weights (α_i), mean values ($\boldsymbol{\mu}_i$) and covariance matrices ($\boldsymbol{P}_i$) of the i-th sub-Gaussian (called "element") are derived through available univariate splitting libraries (Vittaldev et al., 2016), applied to the multivariate distribution related to the orbital state. Specifically, the splitting is performed along a single direction, which is usually chosen as the direction of largest non-linearity or highest uncertainty. In this work, the splitting direction along which the univariate library is applied is considered to be the eigenvector corresponding to the highest eigenvalue of the initial Gaussian covariance to be split. In practice, this translates to exploiting the direction of maximum uncertainty. While multivariate splitting along various directions is necessary for extremely non-linear dynamics, the moderate non-linearity considered in the application of this method justifies the use of univariate splitting, with its general limitations duly noted.

The GMM for the uncertainty representation and propagation is motivated by being a valuable compromise between the Gaussian approximation and the computational demand of MC techniques. Indeed, splitting the initial Gaussian distribution into a GMM results into multiple elements, each provided with a smaller covariance than the original one. This operation enables the shape of the final non-Gaussian distribution to be captured more precisely than with the propagation of the initial Gaussian distribution (Vittaldev et al., 2016). Concurrently, the computational burden is significantly reduced relative to that of a MC propagation of uncertainties, thereby making this stochastic approach valuable when dealing with a cloud of objects (eg: fragments) and their trajectories in time. It should be noted that this statement is only applicable in circumstances where the results and accuracies are equivalent. In fact, a MC analysis with a very small number of samples may be faster than the GMM method, but would yield less accurate results.

The splitting process mentioned above is applied on both parent and fragment Gaussian distributions at initial epoch. Thus, the obtained mean states and covariance matrices are propagated over time exploiting the Unscented Transform (UT) (Julier et al., 2000) approach, due to its accuracy in capturing non-linearities, besides the computational simplicity and speed.

2.1.2. Fragmentation epoch estimation

The epoch detection approach is outlined in the following series of steps. Initially, a set of candidate fragmentation epochs is obtained by computing the epochs of the parent passage through the MOID, for all combinations of the mean state elements of parent and fragment distributions (retrieved by the application of GMM). These epochs are then refined to compute candidate Time of Closest Approach (TCAs). The collision probability between parent and fragment elements is introduced as a criterion to identify the periodicity at which the fragmentation is most likely to have occurred. Finally, the median value and the Median Absolute Deviation (MAD) are determined for the selected set of TCAs. This couple of values provides ultimate information on the estimated event epoch. These steps are detailed in the following paragraphs *Candidate TCAs computation* and *Best TCAs selection*.

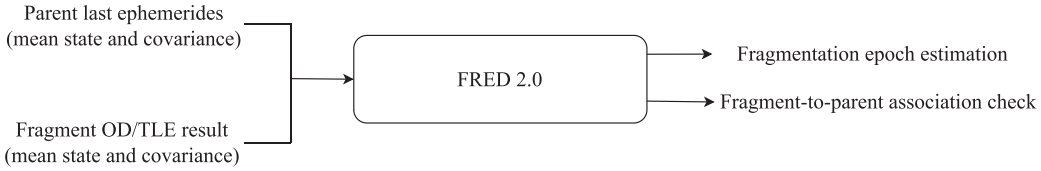

Fig. 2. General flow chart of the epoch estimation algorithm of FRED 2.0.

2.1.2.1. Candidate TCAs computation. The first block in the algorithm (Fig. 3) computes a set of candidate epochs of possible encounters for each element i_p of the parent mixture ($\left\{\boldsymbol{x}_{i_p}^{p}, \boldsymbol{P}_{i_p}^{p}\right\}$) and for each element i_f of the fragment mixture ($\left\{\boldsymbol{x}_{i_f}^{f}, \boldsymbol{P}_{i_f}^{f}\right\}$). These are derived from the application of the GMM splitting, as described in Section 2.1.1.

N_p Gaussian Mixture Elements (GMEs) from the parent mixture and N_f GMEs from the fragment mixture are so generated, resulting in at most $N_p \times N_f$ candidate fragmentation epochs as output. Specifically, these are obtained as the epoch of passage through the MOID location for the parent, whose ephemeris is deemed to be more reliable than the fragment state, as the latter comes from an OD process. This epoch is obtained through an analytical computation of the MOID and is subsequently refined through the iterative process including perturbations presented in (Montaruli et al., 2023b).

The portion of the algorithm is structured as follows:

1. The time window $\left[t_{eph}, t_a\right]$ is sampled with frequency $1/T_p$, where T_p is the parent orbital period computed from the input ephemeris. This results in N_{orb} number of epochs t_i, each related to the i-th periodicity. This frequency is selected as opposed to a $2/T_p$ sampling, since the objective is typically to identify a single minimum distance value, in order to ascertain only one possible encounter among the two occurring in an orbital period.
2. In order to include the state uncertainty in the event epoch identification, N_p GMEs and N_f GMEs are generated through the splitting approach described in Section 2.1.1. In particular, the mean state vectors $\boldsymbol{x}_{i_p}^{p}$ with $i_p = 1, \ldots, N_p$ and $\boldsymbol{x}_{i_f}^{f}$ with $i_f = 1, \ldots, N_f$ are produced.
3. A nested loop is started for each parent GME and fragment GME.

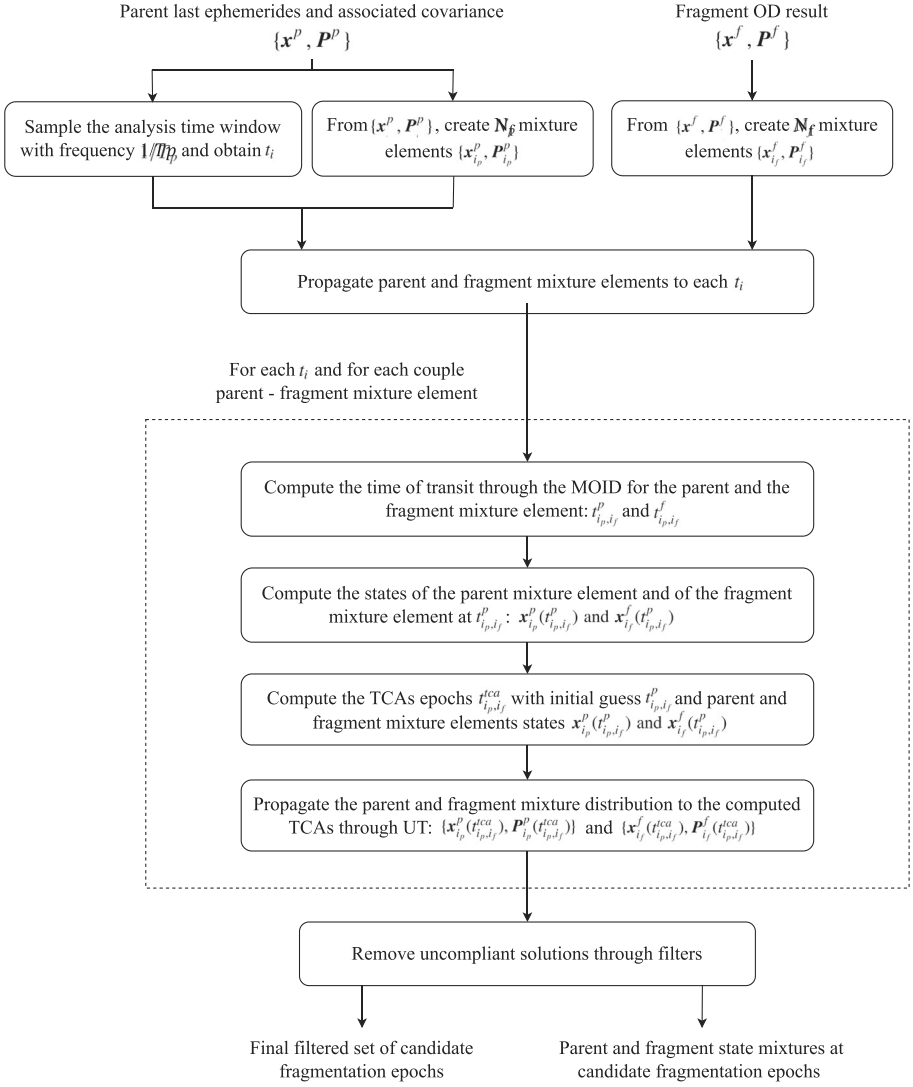

Fig. 3. Flow chart of the epoch estimation algorithm (detail on candidate TCAs computation) of FRED 2.0.

(a) The mean states of parent and fragment elements are propagated to each t_i.

(b) For each t_i, the MOID between the parent element i_p and fragment element i_f, as well as the epochs of transit through the MOID inertial point, are computed analytically, according to (Gronchi, 2002) and leveraging Kepler's equation. The results are indicated as $t^p_{i_p,i_f}$ and $t^f_{i_p,i_f}$. The state vectors $\boldsymbol{x}^p_{i_p}$ and $\boldsymbol{x}^f_{i_f}$ are propagated (possibly including perturbations) up to $t^p_{i_p,i_f}$ and $t^f_{i_p,i_f}$ respectively, resulting in the orbital states $\boldsymbol{x}^p_{i_p}(t^p_{i_p,i_f})$ and $\boldsymbol{x}^f_{i_f}(t^f_{i_p,i_f})$. At this point, the MOID is analytically evaluated again and the computations of $t^p_{i_p,i_f}$ and $t^f_{i_p,i_f}$ are updated. Both epochs are iteratively modified in this manner until, between two consecutive steps, they do not change anymore (according to a tolerance set equal to $1e-03$ s). This iterative cycle is taken from (Montaruli et al., 2023b) and is performed to include the perturbations that are instead not considered in (Gronchi, 2002) formulation, which relies on a purely analytical model. This iterative process results in N_{orb} couples of $\left(t^p_{i_p,i_f}, t^f_{i_p,i_f}\right)$ and $\left(\boldsymbol{x}^p_{i_p}\left(t^p_{i_p,i_f}\right), \boldsymbol{x}^f_{i_f}\left(t^f_{i_p,i_f}\right)\right)$, for the current element i_p and i_f of the mixtures.

(c) The fragment i_f state vector $\boldsymbol{x}^f_{i_f}(t^f_{i_p,i_f})$ is propagated up to the epoch of transit of the parent element i_p through the MOID, resulting in $\boldsymbol{x}^f_{i_f}(t^p_{i_p,i_f})$. This is selected rather than the time of the fragment element i_f transiting through the MOID, on account of the higher reliability associated with the parent ephemeris.

(d) The epochs of the parent element i_p transiting through the MOID $\left(t^p_{i_p,i_f}\right)$ are refined, exploiting the orthogonality between the relative position and the relative velocity between the orbital states of each parent and fragment GME at that epoch ($\boldsymbol{x}^p_{i_p}(t^p_{i_p,i_f})$ and $\boldsymbol{x}^f_{i_f}(t^p_{i_p,i_f})$), according to Eq. 2.

$$\boldsymbol{r}_{rel}(t) \cdot \boldsymbol{v}_{rel}(t) = 0 \tag{2}$$

In the specific instance of the developed algorithm, Eq. 2 is optimized to compute the TCA. To this end, the epoch $t^p_{i_p,i_f}$ is used as first guess. This process allows to obtain in output accurate candidate TCA epochs, in number N_{orb} (one for each periodicity). At this point the parent and fragment GMEs ($\left\{\boldsymbol{x}^p_{i_p}, \boldsymbol{P}^p_{i_p}\right\}$ and $\left\{\boldsymbol{x}^f_{i_f}, \boldsymbol{P}^f_{i_f}\right\}$) are propagated through an UT function to the refined TCA, which represents the fragmentation candidate epochs.It is important to acknowledge that the MOID is a purely geometric parameter, contingent solely on the orbits of the two objects. Being time independent, it does not provide information on the actual relative positions of the objects. Consequently, the TCA epochs, as delineated in this study, facilitate the incorporation of the temporal variable into the problem. This, in turn, enables the determination of the epochs during which the encounter may have occurred in reality.

4. The points above previously mentioned are reiterated for all possible combinations of N_p times N_f elements, which results in a number $N_{orb} \times N_p \times N_f$ of evaluations. To eliminate unfeasible solutions, a filtering phase is adopted, as outlined below. The first filter requires that the couples with combinations (i_p, i_f) for which the value $t^{tca}_{i_p,i_f}$ is not included in the boundaries of the time window $\left[t_{eph}, t_a\right]$ are eliminated. With the second filter, for each t_i, the couples with combinations (i_p, i_f) for which $t^{tca}_{i_p,i_f} < \left(t_i - T_p/2\right)$ or $t^{tca}_{i_p,i_f} > \left(t_i + T_p/2\right)$ are filtered out. In this way, the passage epochs that, despite being calculated at the i-th periodicity, fall beyond t_i plus or minus a semi-period, are eliminated. The next filter is based on a Density-Based Spatial Clustering of Applications with Noise (DBSCAN) (Ester et al., 1996), applied to eliminate couples with combinations (i_p, i_f) which are considered outliers (setting the maximum time deviation to 5 min). Lastly, the final filter requires that the miss distance, related to the computed TCAs, shall be lower than a certain threshold. Consequently, epochs that are not actually feasible in representing a close approach are discarded. From this point forward, the number of GME elements (N_p and N_f) is going to be referred to the updated count of $t^{tca}_{i_p,i_f}$ which have not been discarded by the filters.
5. In the event that, subsequent to the filtration process, the $t^{tca}_{i_p,i_f}$ related to all combinations $\left(i_p, i_f\right)$ are not compliant for all N_{orb} periodicities, the fragment under analysis is discarded. Therefore, it is acknowledged that an analysis involving a fragment can provide no result. This is attributable to the precision of the orbital states, and the rejection of such data enables the prevention of erroneous evaluations.

2.1.2.2. Best TCAs selection. The second block of the routine (Fig. 4) aims to finally detect the epoch of the fragmentation event, given the parent-fragment couple under analysis. The inputs are obtained from the previous portion of the algorithm (Fig. 3) and and are thus processed using a collision risk assessment metric. Specifically, the event under analysis is treated as a conjunction between a primary object (the parent) and a secondary object (the fragment). This approach facilitates the evaluation of the Probability of Collision (PoC) values at the fragmentation epoch candidates and the identification of the periodicity where the PoC value is highest. This, in turn, provides an initial insight into the epoch in which the encounter is most likely to have occurred.

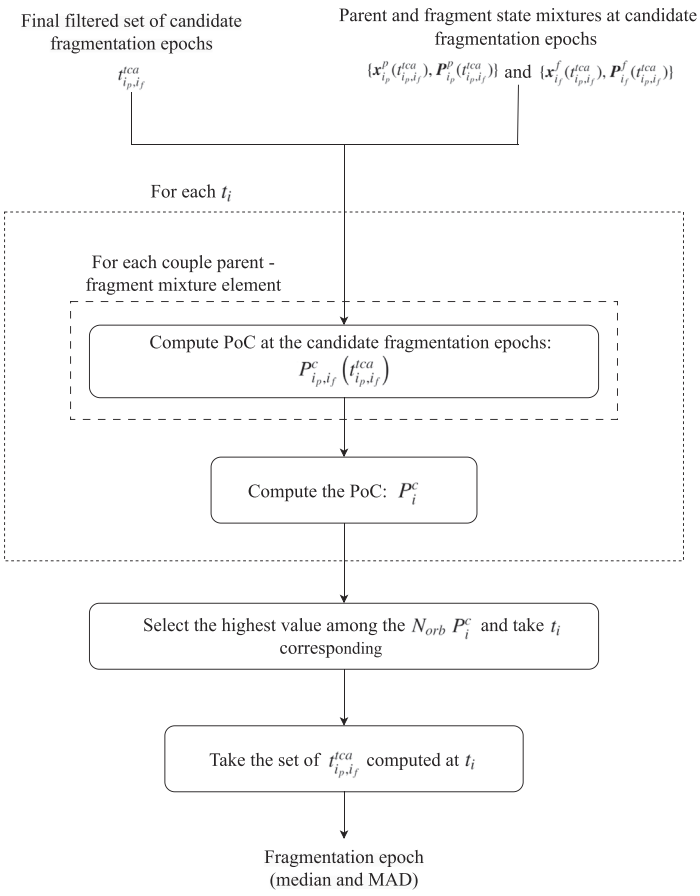

Fig. 4. Flow chart of the epoch estimation algorithm (detail on candidate TCAs ranking) of FRED 2.0.

The inputs required for this portion of the algorithm are the refined candidate TCA epochs at all periodicities and for all combination of GMM elements ($N_{orb} \times N_p \times N_f$ values of $t^{tca}_{i_p,i_f}$). The mean states and covariance matrices of parent and fragment GMEs at these epochs are also required ($\left\{\boldsymbol{x}^p_{i_p}\left(t^{tca}_{i_p,i_f}\right), \boldsymbol{P}^p_{i_p}\left(t^{tca}_{i_p,i_f}\right)\right\}, \left\{\boldsymbol{x}^f_{i_f}\left(t^{tca}_{i_p,i_f}\right), \boldsymbol{P}^f_{i_f}\left(t^{tca}_{i_p,i_f}\right)\right\}$). This second portion of the routine is structured as follows:

1. A nested loop is started for each parent and fragment GME.
2. For each t_i, the PoC between the current parent and fragment GMEs is computed, through Chan's method (Chan, 2008). The inputs entering the PoC computation are the mean values and covariance matrices of the GMEs distributions $\left\{\boldsymbol{x}^p_{i_p}\left(t^{tca}_{i_p,i_f}\right), \boldsymbol{P}^p_{i_p}\left(t^{tca}_{i_p,i_f}\right)\right\}, \left\{\boldsymbol{x}^f_{i_f}\left(t^{tca}_{i_p,i_f}\right), \boldsymbol{P}^f_{i_f}\left(t^{tca}_{i_p,i_f}\right)\right\}$ at the corresponding candidate TCA epochs. The Hard Body Radius (HBR), that is the sum of the radii of the spheres containing the two objects, is also required. Nevertheless, it is important to notice that, in the case of a fragmentation event analysis, any value employed for the HBR lacks of a physical meaning. Indeed, before the event the fragment was a part of the parent object, and the sum between their radii has no physically meaning. To address this issue, in this algorithm, the combined HBR is set equal to the radius of the sphere equivalent to the relevant dimension of the parent object, which is assumed to be already known, given that the parent is a catalogued object.
3. For a certain combination (i_p, i_f), N_{orb} collision probabilities are obtained, as $P^c_{i_p,i_f}\left(t^{tca}_{i_p,i_f}\right)$.
4. To agglomerate, for each periodicity, the values of PoC computed for all the GMEs combinations, the formulation proposed by Vittaldev in (Vittaldev et al., 2016) and reported in Eq. 3 is applied:

$$P^c = \sum_{i_p=1}^{N_p}\sum_{i_f=1}^{N_f} \alpha_{i_p}\alpha_{i_f} f_{\mathrm{PoC}}\left\{\boldsymbol{x}^p_{i_p}\left(t^{tca}_{i_p,i_f}\right), \boldsymbol{P}^p_{i_p}\left(t^{tca}_{i_p,i_f}\right), \boldsymbol{x}^f_{i_f}\left(t^{tca}_{i_p,i_f}\right), \boldsymbol{P}^f_{i_f}\left(t^{tca}_{i_p,i_f}\right), \mathrm{HBR}\right\} \tag{3}$$

Here f_{PoC} denotes the function used to compute the PoC value (which in this work is represented by Chan's method (Chan, 2008)), while α_{i_p} and α_{i_f} correspond to the weights of each GMM element for parent and fragment objects respectively, computed through the splitting library mentioned in Section 2.1.1. The PoC value f_{PoC} is computed in the encounter reference frame, with center in the primary object (the parent). Therefore, all quantities at TCA appearing in Eq. 3 are projected in the encounter plane. A short-term method is selected for the collision probability computation instead of a long-term one, in order to derive an instantaneous value

of the PoC, as required by the Vittaldev approach.Overall, one value of PoC per periodicity is therefore derived, and denoted as P_i^c with $i = 1, \ldots, N_{orb}$.

5. In order to detect a time interval in which it is possible that the fragmentation event occurred, the highest PoC criterion is applied. This is achieved by selecting the maximum value among the N_{orb} P_i^c values. The set of $N_p \times N_f$ TCA epochs t_{i_p,i_f}^{tca} corresponding to the periodicity where the highest PoC value is found is retained as $\tilde{t}_{i_p,i_f}^{tca}$, while the others are discarded.
6. The ultimate objective is to provide the final result on the estimated fragmentation epoch. In order to do so, statistical values, such as median and Median Absolute Deviation (MAD) of the final time distribution are derived, to provide a measure of the "quality" of the result and its uncertainty (see Section 3.3). It is worth pointing out that the resulting fragmentation epoch distribution cannot be assumed as Gaussian and, for this reason, median and MAD are preferred rather than mean and standard deviation to measure the quality of the estimated fragmentation epoch, and its uncertainty. The median value (Huber, 2004) is the value that separates the higher half of a distribution from the lower half. It is of central importance in robust statistics and used in this case since it is not affected by the skewness of the distribution, and therefore provides a more reliable representation of its center. Indeed, as mentioned, the results of the method, denoted as $\tilde{t}_{i_p,i_f}^{tca}$, do not necessarily constitute a Gaussian distribution. Consequently, the use of the mean value would not be as reliable. Eq. 4 is therefore applied.

$$\tilde{t}_{event} = \text{median}\left(\tilde{t}_{i_p,i_f}^{tca}\right) \quad \forall i_p \text{ and } \forall i_f \text{ in } N_p, N_f \tag{4}$$

Furthermore, to quantify the uncertainty, the MAD (Huber, 2004) of the final epochs is evaluated. The MAD is the median value of the absolute values of the residuals with respect to the data median. It is used in robust statistics, since it is more resilient to outliers than the standard deviation. Hence, the MAD is a better statistical measure to exploit when dealing with distributions without a mean or variance, such as in this case non-symmetric and non-Gaussian distributions. Indeed, Eq. 5 is applied.

$$\tilde{u}_{event} = \text{MAD}\left(\tilde{t}_{i_p,i_f}^{tca}\right) \quad \forall i_p \text{ and } \forall i_f \text{ in } N_p, N_f \tag{5}$$

2.1.3. Using FRED 2.0 to associate fragments to parent

As mentioned in Section 1, FRED 2.0 has been developed also to address the issue of associating an uncatalogued object to a fragmentation event. The only assumption is that the fragmentation of a given parent object has been detected.

In order to establish whether an uncatalogued object can be associated with the satellite that broke-up, a measure of total collision probability is employed within the analysed time window. Specifically, if the probability of at least one encounter occurring within the time span exceeds a certain threshold, then the association is considered positive, regardless of the accuracy of the estimated fragmentation epoch. This measure of the total probability in time is referred to as P_{tot}^c.

The following procedure was developed to evaluate it:

1. The candidate sets of TCA epochs, which are associated with the potential close encounters along the time periodicities, are computed in accordance with the methodology outlined in paragraph *Candidate TCAs computation* (Section 2.1.2.1).
2. The PoC of each encounter at the related set of TCA epochs (P^c) is computed, through Eq. 3.
3. The probability that the encounter considered in the previous step does not occur is defined as $(1 - P^c)$.
4. By repeating point 2 for the all N_{orb} values of P^c (all encounters), and by evaluating their product as in Eq. 6, the probability of no encounters happening within the considered time window is retrieved.

$$\Gamma = \Pi_{i=1}^{N_{orb}} \left(1 - P_i^c\right) \tag{6}$$

5. The probability that at least one encounter between the two objects occurs in the entire time window can be now evaluated as:

$$P_{tot}^c = 1 - \Gamma.$$

Following the computation of the total probability of encounter occurrence (P_{tot}^c), a comparison of the result with a threshold is then made. Should the value fall below this threshold, the association of the fragment body to the primary object is deemed negative. Conversely, if the value exceeds the threshold, it can be concluded that the observed object is a product of the parent break-up. The determination of this threshold can be facilitated through numerical simulations, by applying the outlined approach to a set of fragments simulated through the break-up model for the event under consideration. The resulting P_{tot}^c values are then examined to identify the least conservative value (the smallest), which is then designated as the threshold. It is important to note that the propagation scenario (Keplerian or SGP4 model (Vallado et al., 2006)) has a significant influence on the outcome of the selected threshold.

The association procedure is thus included in the routine, which is summarized in the block diagram in Fig. 2.

2.2. An operational technique to derive a covariance from TLEs

As previously mentioned, the inputs of the algorithm are the mean orbital states of the parent and the fragment objects, along with their associated covariance matrices. However, it should be noted that in certain cases, the input

ephemerides may only be available in a deterministic format, such as the TLE format. In these operational cases, it becomes essential to determine a realistic covariance matrix, and, to this end, the approach described in (Osweiler, 2006) can be used both for the parent and fragment objects. The approach to estimate a covariance matrix $\overline{\boldsymbol{P}}$ at a certain epoch $\bar{t}$ is here summarized:

1. The epoch of interest $\bar{t}$ is referred to as "primary" epoch.
2. A number $\hat{N}$ of "secondary" TLEs is retrieved up to an arbitrary number of days before (or after) $\bar{t}$ epoch.
3. Each of the secondary TLEs states is propagated forward (or backward) in time, up to $\bar{t}$, through SGP4 (Vallado et al., 2006).
4. For each secondary TLE, the residual at $\bar{t}$ is computed:

$$\delta \boldsymbol{x} = \hat{\boldsymbol{x}} - \bar{\boldsymbol{x}}$$

between secondary ($\hat{\boldsymbol{x}}$) and primary ($\bar{\boldsymbol{x}}$) state vectors. In general, $\boldsymbol{x}$ refers to the vector gathering the orbital characteristics, which can be the cartesian state or the Keplerian elements, for example.
5. The mean of the obtained $\hat{N}$ residuals is computed, and here called $\boldsymbol{\mu}_{\delta \boldsymbol{x}}$.
6. The covariance is generated through the sample covariance definition:

$$\overline{\boldsymbol{P}} = \frac{\sum_{i=1}^{\hat{N}} (\delta \boldsymbol{x}_i - \boldsymbol{\mu}_{\delta \boldsymbol{x}})(\delta \boldsymbol{x}_i - \boldsymbol{\mu}_{\delta \boldsymbol{x}})^T}{\hat{N}}$$

In the case of the present study, this approach is applied only to associate a covariance to the parent object. Indeed, multiple orbital states of the satellite are required to compute the covariance, and this prevents from applying it to the fragment in the first epochs after the break-up, that is in the operational framework of both FRED and FRED 2.0 algorithms. Thus, the covariance associated to the fragment orbital state is considered as returned by the orbit determination process.

3. Numerical simulations

The present section is intended to analyse the outcomes obtained by applying FRED 2.0 to a simulated test case, with the objective being to evaluate its performance and robustness across different propagation models and scenarios. All numerical simulations have been executed in MATLAB (MathWorks, 2023), together with functions from NASA SPICE Toolkit (NASA-JPL, 2023), on a single core with Intel(R) Core(TM) i7-8565U CPU @ 1.80 GHz 1.99 GHz processor.

The conditions of the nominal test scenarios as well as those of the sensitivity analyses are intentionally maintained analogous to those employed in (Montaruli et al., 2023c), with the objective of enabling a comparison between FRED 2.0 and the original FRED version.

3.1. Simulation data

This section delineates the preparation of the simulations conducted to test the algorithms described in Section 2, in terms of input data and parameter settings.

3.1.1. Test case description

The analysed fragmentation scenario is a past event involving a kinetic Anti-Satellite Test (ASAT) occurred around 02:47 UTC on November 15th, 2021 (Muciaccia et al., 2023). This event led to the destruction of a Russian satellite, named Cosmos-1408. As of June 20, 2022, the U. S. Space Surveillance Network had catalogued a total of 1,764 objects, 806 of which remained in orbit, according to recent analyses (Pardini and Anselmo, 2023). These numbers make this ASAT test the third most severe fragmentation event recorded to date, after Fengyun-1C ASAT test and Cosmos-2251 collision with Iridium-33.

The orbital elements of Cosmos-1408 derived from the last available TLE are reported in Table 1. It is worth to remark that, for the purposes of this preliminary analysis, the ballistic coefficient set in SGP4 propagation is equal to zero, thereby neglecting the parent orbital decay. A further simulation is then carried out in Section 3.4.4, employing a more realistic B* value. The corresponding position and velocity state vectors at epoch t_{eph} are reported in Table 2, and considered as the last available parent object orbital state in the simulation. The fragmentation epoch is searched for in an analysis time window that ranges from t_{eph} up to an epoch close to the time when the alert of the event was provided, that is 06:00 UTC on November 15th.

3.1.2. Parent covariance generation

As described in Section 2, together with the ephemeris of the parent object, a covariance matrix representing the uncertainty in the state knowledge is required. This covariance is generated through the operational procedure proposed in Section 2.2. In the test case conducted within this work, TLEs are considered as the available deterministic information for the parent object (Space-Track, 2023) and the state vector employed to compute the residuals is the Cartesian one, containing the position and velocity. In particular, it is assumed that the parent state vector is available from the last catalogued TLE before the event. The method described in Section 2.2 is therefore applied exploiting a number of $\hat{N} = 5$ TLEs, previous with respect to t_{eph} (the epoch of the last available TLE), downloaded from the Space-Track website (Space-Track, 2023). The number of past TLEs, extending up to 5 days prior to

Table 1
Cosmos-1408 Keplerian elements at t_{eph}: 2021–11-14 23:20:00.00 UTC.

a [km]	e [–]	i [deg]	Ω [deg]	ω [deg]	M [deg]	B*
6862.2	0.003	82.7	123.4	91.9	254.90	0

Table 2
Cosmos-1408 TLE epoch and corresponding state vector at t_{eph}: 2021–11-14 23:20:00.00 UTC.

$\boldsymbol{r}^p$ [km]	−3812.229	5692.616	379.691
$\boldsymbol{v}^p$ [km/s]	−0.5645	−0.9086	7.5467

the primary epoch, has been selected in order to avoid generating an unrealistically large covariance matrix.

The described approach is thus applied to the parent state reported in Table 2. The numeric result of the covariance matrix generation is reported in Section 3.2, and the corresponding GMM distribution is represented before and after a propagation in time (Fig. 6a Fig. 6b, respectively), showing the benefits in capturing the generated shape for the parent covariance matrix.

3.1.3. Fragments data set generation

The fragments data set is also prepared prior to the simulations. This step involves the application of a break-up model to generate simulated orbital states of the fragments, their subsequent virtual detection to obtain measurements and an OD algorithm to reconstruct their orbits in terms of mean state and covariance.

3.1.4. Fragmentation event simulation

A set of fragments orbital state vectors are first generated by applying the NASA Standard Break-up Model (SBM) (Johnson et al., 2001), simulating the velocity impulses imparted to the debris. This process is summarized below.

1. The parent state vector $\boldsymbol{x}^p = \{\boldsymbol{r}^p, \boldsymbol{v}^p\}^T$, dated at t_{eph}, is propagated up to t_0: 02:47:00 UTC on November 15th.
2. The fragmentation event is modeled as a set of velocity impulses applied to the satellite orbital state at t_0, according to the SBM equations (Johnson et al., 2001).
3. A set of 237 fragments is generated in such way.
4. At t_0, the pericentre radius of each fragment is evaluated. Those with a pericentre altitude less than 120 km are discarded because they are expected to re-enter, and are not used in the routine testing. This reduces the data set to 229 when the Keplerian model is used to propagate the simulated fragments, and 226 fragments when SGP4 (Vallado et al., 2006) is exploited.

3.1.5. Fragments detection

The obtained ephemerides of the fragments are propagated until epoch t_{od}, obtaining $\boldsymbol{x}^f(t_{od})$, when a surveillance radar detection is simulated, and the orbital states and covariance matrices $\{\boldsymbol{x}^f, \boldsymbol{P}^f\}$ are determined. Nominally, t_{od} is set to 13 h after the fragmentation event, since FRED 2.0 aims to exploit a single fragment observation result, available a few hours after the event. The approach to simulate the determination process is different depending on the scenario analysed, and it is described below.

- *Scenario with no OD error*In this case, a fixed covariance matrix (with standard deviations on position and velocity of respectively $9.32e-05$ km and $1.38e-06$ km/s) is simply associated to all fragments. The matrix is derived through the same IOD approach detailed in the point below (*Scenario with OD error*), setting in this case low values for the measurement noise. This approach results in a small value of the covariance trace, and as a consequence, in positional and velocity uncertainties which are compatible with a near ideal IOD process. The final output is a unique mean state $\boldsymbol{x}^f$ for each fragment, and a constant covariance matrix $\boldsymbol{P}^f$ for all of them.
- *Scenario with OD error*In this case the fragment mean state $\boldsymbol{x}^f(t_{od})$ is propagated in the measurement time window $[t_{od}, t_{od}+30\text{s}]$. The resulting propagated states are projected into the measurements space to derive a set of simulated angular and range measurements. Subsequently, a standard noise is applied on the range measurement and its standard deviation is set to 30 m. The angular noise is considered equal for both azimuth and elevation and its standard deviation is set to 0.01° in the nominal scenario. These values have been selected consistent with the characteristics of a radar survey sensor (Montaruli et al., 2024c). The Doppler shift is not considered as a measurement for this simulation. A radar IOD process is then simulated according to the Keplerian-based method presented in (Siminski, 2016), to obtain a first estimate of the state and covariance matrix of each fragment. The obtained results are refined through the Refined Orbit Determination (ROD) function presented in (Montaruli et al., 2022), based on an Unscented Kalman Filter (UKF), and exploiting a non Keplerian dynamics model in the perturbed scenario. The final output is hence a unique couple of mean state and uncertainty covariance for each single fragment, both in position and velocity ($\{\boldsymbol{x}^f, \boldsymbol{P}^f\}$).

In the original version of FRED tool the data set related to the fragment objects is generated by applying only the IOD process on the simulated measurements which exploits the Keplerian-based method in (Siminski, 2016). The IOD result is hence not refined through an ROD algorithm, as instead occurs in the simulations conducted on FRED 2.0. This must be taken into account when comparing the performance of the epoch estimation algorithm of the original FRED tool with that of FRED 2.0.

3.1.6. Fragment-to-parent association data set

Space objects unrelated to the event are considered as well, with the aim of testing the capability of FRED 2.0 fragment-to-parent association algorithm in avoiding wrong associations. The objective is to achieve the validation of a robust approach capable of discarding false associations of non-related RSOs, particularly those that are in close proximity to the location, epoch or regime of the frag-

mentation event. To this end, the Space-Track catalogue (Space-Track, 2023) is utilized to download TLEs of generic near-Earth objects, and their ephemerides are employed to validate the association approach.

Following the completion of the download process, the catalogued objects are subjected to a screening procedure that aligns with the methodology outlined in (Bonaccorsi et al., 2024). In the context of the tested scenario, 45,993 objects have been downloaded. The catalogue screening tool is utilized to filter the objects, resulting in a final count of 105. For these objects, fictitious measurements are generated from a virtual ground-station and with noise, and processed through the same IOD and ROD algorithms mentioned in Section 3.1.5. The results are then input to the fragment-to-parent association method presented in Section 2.1.3, as they represented "false" fragments to be tested against the parent object.

3.1.7. Other input data

All remaining inputs to run the routine can be therefore defined: the analysis time window ranges from t_{eph} (2021–11-14 23:20:00 UTC) to t_a (2021–11-15 06:00:00 UTC), the number of GMEs for the parent and fragment objects is set to $N_p = 9$ and $N_f = 9$ respectively. The analysis time window is approximately 6.7 hours long; since the parent orbital period computed at t_{eph} is equal to about 1.6 h, N_{orb} results equal to 5. Furthermore, the combined HBR is set equal to the parent HBR, which is fixed to 2.5 m, that is equal to the radar cross section associated to Cosmos-1408 (LeoLabs, 2021). Finally, the threshold on the lower bound of P^c_{tot} for a positive fragment-parent association, described in Section 2.1.3, is set equal to 10^{-9} when the propagation occurs through a Keplerian model, while 10^{-10} otherwise. These thresholds are obtained from tests performed with the simulated settings described above, by applying only the fragment-to-parent association method to the fragments data set and evaluating the results. The considered fragments data set corresponds to the scenario with OD error (Section 3.1.5), using both the Keplerian and the SGP4 models, from which the two thresholds are derived, respectively. The results for two tests are reported in Fig. 5. From the tests, the most conservatives values for the association threshold on P^c_{tot} result to be 10^{-9} (Keplerian propagation) and 10^{-10} (SGP4 propagation).

3.2. GMM test case

The graphical outcomes of the GMM generation for the parent object are hereby presented, with the objective of verifying the representation of the distribution subsequent to propagation over time.

Firstly, as mentioned in Section 3.1.2, the tool described in Section 2.2 is applied to generate the covariance matrix associated to the parent object at epoch t_{eph}. The results of the tested approach is here reported in Eq. 7, named as $\boldsymbol{P}^p$.

$$\boldsymbol{P}^p = \begin{bmatrix} 0.0096 & 0.0045 & -0.0849 & -5.1358e-05 & 7.8904e-05 & -8.9045e-06 \\ 0.0045 & 0.0024 & -0.0412 & -2.4932e-05 & 3.8243e-05 & -4.6004e-06 \\ -0.0849 & -0.0412 & 0.7549 & 4.5684e-04 & -7.0168e-04 & 8.0220e-05 \\ -5.1358e-05 & -2.4932e-05 & 4.5684e-04 & 2.7646e-07 & -4.2464e-07 & 4.8524e-08 \\ 7.8904e-05 & 3.8243e-05 & -7.0168e-04 & -4.2464e-07 & 6.5224e-07 & -7.4470e-08 \\ -8.9045e-06 & -4.6004e-06 & 8.0220e-05 & 4.8524e-08 & -7.4470e-08 & 8.7990e-09 \end{bmatrix} \quad (7)$$

A set of 5,000 position samples are generated from the initial distribution of the parent orbital state at t_{eph} ($\{\boldsymbol{x}^p, \boldsymbol{P}^p\}$), and then each one is propagated through the Keplerian model for 6.3 h, as would occur with a MC analysis. The 5,000 samples are illustrated as black dots in Fig. 6a at initial epoch and in Fig. 6b after the propagation. In order to facilitate a comparison between the GMM splitting and the MC analysis (which is regarded as the reference), other position samples are generated from the mixtures. These are derived as random multivariate distributions from the N_p GMEs of the parent object at epoch t_{eph}, derived from the splitting of the Gaussian covariance $\boldsymbol{P}^p$. Similarly, Fig. 6b shows the samples generated from the same GMEs and propagated through UT (with Keplerian model), up to 6.3 h (corresponding to the last periodicity epoch). As is evident from the plots, the splitting direction computed as explained in Section 2.1.1 works well when applied to the covariance matrix obtained through the method proposed in 2.2. Indeed, the samples generated from $\boldsymbol{P}^p$ (Eq. 7) through the splitting approach demonstrate a strong similarity to the MC samples. At the end of the propagation, the elements of the mixture are capable of

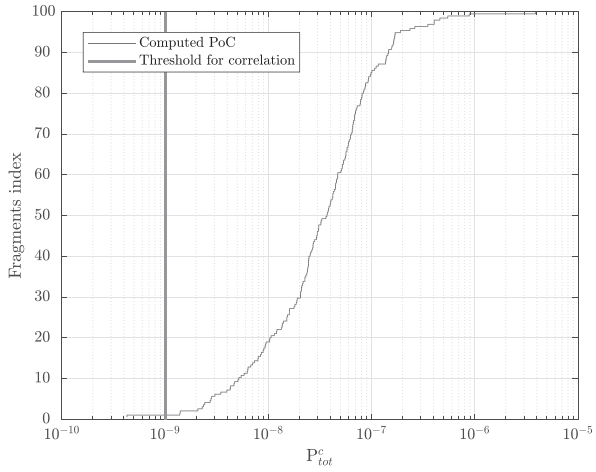

(a) Fragment-to-parent association threshold definition test, conducted on the data set derived with OD error and Keplerian dynamics.

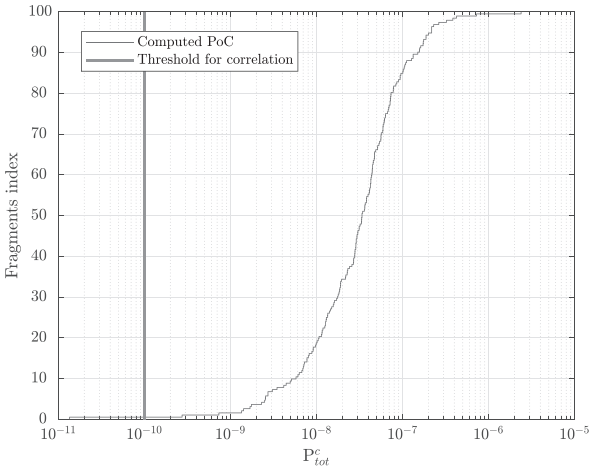

(b) Fragment-to-parent association threshold definition test, conducted on the data set derived with OD error and SGP4 dynamics.

Fig. 5. Tests conducted in the scenario with OD error in order to define the fragment-to-parent association threshold on the total PoC value. The plots report the cumulative density function of the P^c_{tot} value, in logarithmic scale, used to verify the association. As observed in (a), with a Keplerian dynamics, almost the entire data set has P^c_{tot} values which overcome approximately the order of 10^{-9}, highlighted by the vertical darker line. In (b), when applying a perturbed dynamics through SGP4, the values tend to decrease of an order of magnitude, and the lowest value for a positive fragment association is approximately 10^{-10}, highlighted by the vertical darker line.

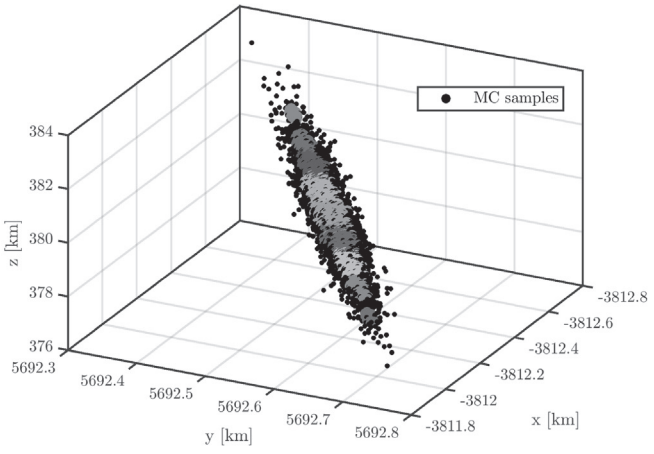

(a) Parent object GMEs (derived from $\boldsymbol{P}^p$) and MC samples at t_{eph}.

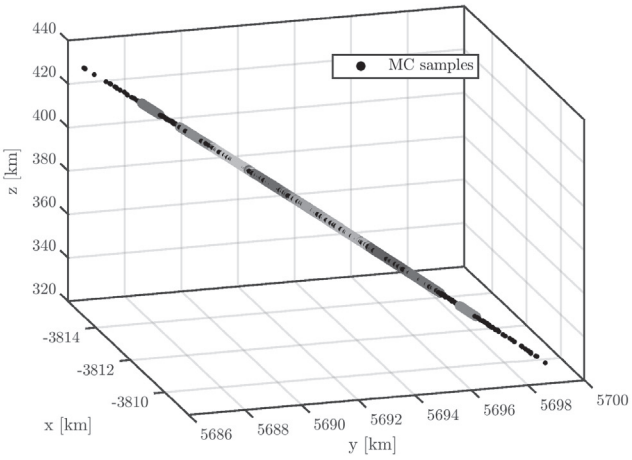

(b) Parent object GMEs and MC samples after 6 h propagation.

Fig. 6. Uncertainty of the parent covariance in Earth-centered inertial frame. Comparison between the representation according to a MC distribution and to GMM one. The two representations are reported at initial epoch and after 6.3 h propagation, through the Keplerian model. It can be seen that the GMEs generated through the splitting strategy mentioned in Section 2.1.1 well describe both the initial and the final distribution of uncertainty, particularly when compared to the shape of the MC samples considered here as the reference for uncertainty propagation.

capturing the curvature along the long-track direction, generated by the dynamics.

3.3. Simulations results

Simulations have been conducted on the entire population of fragments from the data set generated as described in Section 3.1, facilitating the post-process of the results.

The assessment of the goodness of the results, and consequently the performance of the method, is accomplished through the use of the median and the MAD, as described in Section 2.1.2.2. The error values associated with the set of TCAs resulting from the method are defined in Eq. 8. Together with the median value computed through Eq. 9, an uncertainty measure of the errors is also provided, as in Eq. 10.

$$\varepsilon = \tilde{t}^{tca}_{i_p,i_f} - t_0 \forall i_p \text{and} i_f \text{in} N_p, N_f \quad (8)$$

$$\tilde{\varepsilon} = \text{median}(\varepsilon) \forall i_p \text{and} i_f \text{in} N_p, N_f \quad (9)$$

$$\tilde{u}_\varepsilon = \text{MAD}(\varepsilon) \quad (10)$$

Each epoch estimation is considered correct if either one of these two cases occurs:

- The median value of the error between the estimated epoch and the actual time of the event (Eq. 9), in absolute value, is lower than three minutes ($|\tilde{\varepsilon}| \leqslant 3\ min$).
- The median epoch among the TCAs is erroneously estimated ($|\tilde{\varepsilon}| > 3\ min$), but the uncertainty is wide enough to include such an error, and this makes the computed epoch estimation statistically compliant. From a mathematical point of view, it occurs that $|\tilde{\varepsilon}| > 3min$ and $|\tilde{\varepsilon}/\tilde{u}_\varepsilon| \leqslant 3$.

The three-minute threshold is determined by starting from the same metric of one minute used in the reference work (Montaruli et al., 2023b). The value is then multiplied by 3 (in what can be termed a 3σ representation) in order to enhance the flexibility of the evaluation and ensure its relevance to operational scenarios.

For all fragments that do not yield a correct estimation, two categories can be identified:

- Computation fails: this is the case occurring when, even though convergence to the correct periodicity is achieved, the median error remains higher than the threshold, and the incorrect epoch estimation is not mitigated by its uncertainty. This hence occurs: $|\tilde{\varepsilon}| > 3min$ and $|\tilde{\varepsilon}/\tilde{u}_\varepsilon| > 3$. This type of failure emerges when the TCA distribution is close to the correct periodicity but clusters around a point significantly distant from the fragmentation epoch. This failure may be caused by inaccurate estimates of the MOID transit epoch, which consequently provide inaccurate first guesses for the calculation of TCAs.
- Ranking fails (A): this is the case where convergence to the correct periodicity is not achieved, as the time error is larger than half of the parent orbital period. However, the ratio between the median error with respect to the closest periodicity epoch and its dispersion (MAD) is lower than 3. This results in an erroneous fragmentation epoch, yet the time error is a multiple of the periodicity. This means that the epoch of the fragmentation event is wrongly estimated, but the inertial position of the breakup can be correctly computed. This information can be instrumental in the planning of observational campaigns aimed at cataloguing the fragments generated by the event.
- Ranking fails (B): in this case the convergence to the correct periodicity is not achieved and the ratio between the median error with respect to the closest periodicity epoch and its dispersion (MAD) is larger than 3. In this case both the epoch and the inertial position of the fragmentation event are erroneously estimated.

3.3.1. Unperturbed scenario, no OD error

The unperturbed scenario without any OD orbital state error is tested to assess the theoretical performance of the routine. By "unperturbed," it is meant that the propagation of the objects in time, both in the generation of the data set and within the algorithms detailed in Section 2.1, occurs through an analytical Keplerian model, without the addition of perturbations. For the generation of all the required inputs, for both the parent object and fragments, the approaches described in Section 3.1.2 and in Sec: 3.1.5, are applied before running the simulation.

In this case 229 fragments "survived" the filters on the pericenter altitude, on the candidate epochs and on the Distance of Closest Approach (DCA) threshold. The results of the epoch estimation approach, in terms of percentages above defined, are reported in Table 3. As reported in Table 3, the method always estimates the event epoch with a median error lower than three minutes, for all simulated fragments. The median error $|\tilde{\varepsilon}|$ is reported for all non-discarded simulations and in seconds, in terms of percentiles, in Table 4.

It is evident that these are considerably lower than three minutes, with orders of magnitude of the 10^{-1} seconds in the worst case (100th percentile in Table 4). Therefore, under theoretical conditions the method is highly accurate.

The performance of the association process described in Section 2.1.3 are also verified. This is successful for all the fragments simulated for this test case, as reported in Table 5. This occurs because the association criterion is always met, as $P^c_{tot} > 10^{-9}$ for all fragments. The association is also tested against false positives, on the data set of unrelated objects derived from Space-Track catalogue, and the results are shown in the last two columns of Table 5. Indeed, it appears that all objects which passed the catalogue screening and are analyzed through FRED 2.0 return no association, since their value of P^c_{tot} does not overcome the threshold of 10^{-9}. Consequently, the results of this simulation prove the correct working of FRED 2.0 in ideal conditions.

For all 229 fragments, this simulation required a computational time of about 17.5 minutes, that is approximately 4.6 s per fragment. For the same analysis, original FRED algorithm takes 30 s per fragment using 1000 samples (Montaruli et al., 2023c), demonstrating the computational advantage of leveraging a statistical representation based on GMM. However, the following analysis was carried out with a deliberately limited number of GMEs compared to the maximum allowed by the univariate splitting library

Table 3
Unperturbed scenario with no OD error. Epoch estimation results. FRED 2.0 correctly detects the event epoch along all simulated fragments. In fact, in the ideal scenario where no perturbations are introduced into the Keplerian dynamical model and no errors are simulated in the fragment orbit determination process, no failure cases occur.

Correct solutions	Computation fails	Ranking fails (A)	Ranking fails (B)
100 %	0 %	0 %	0 %

Table 4
Unperturbed scenario with no OD error. Median time error percentiles. The epoch estimation is always correctly estimated, as the 100th percentile falls below the three minutes limit. Beyond being correct, the epoch estimation is also accurate, as the percentiles deviate from the true epoch by only a few milliseconds.

Percentiles [seconds]				
5th	25th	50th	75th	100th
0	0	0	3.576e-07	0.124

Table 5
Unperturbed scenario with no OD error. Results of the fragment-parent association process. The percentages of true positives and false negatives represent the number of simulated fragments that are correctly or incorrectly associated with the fragmentation event, respectively. Similarly, the percentages of true negatives and false positives correspond to the proportion of objects, which passed the catalogue screening, that are correctly or incorrectly identified as unrelated to the fragmentation event, respectively. In this scenario, all simulated fragments are correctly associated to the event, while all catalogued and unrelated objects do not satisfy the association threshold.

True positives	False negatives	True negatives	False positives
100 %	0 %	100 %	0 %

Table 6
Unperturbed scenario with no OD error. Comparison with FRED in terms of correct solutions in the epoch estimation and computational time per simulation. Source: (Montaruli et al., 2023c). It can be seen that FRED 2.0 achieves a higher percentage of correct solutions with respect to original FRED, by also reducing the computational burden required for the analysis on a single fragment.

	FRED	FRED 2.0
Correct solutions	92.8 %	100 %
Computational time per fragment	30 s	4.6 s

(that is 39). If the number of mixture elements were increased, longer computational times would need to be taken into account. The comparison in terms of computational time required by the simulations is also reported in Table 6, as well as the number of correct solutions achieved in the epoch detection by both algorithms.

In addition to its computational efficiency, it can be noticed that FRED 2.0 achieves a higher number of correct epochs detection. This enhancement may be attributed to the methodology employed for generating mean state and covariance, which differs in the two algorithms, as explained in Section 3.1.5. However, it should be also considered that the definitions of "Correct" solutions is different between the two methods.

3.3.2. Perturbed scenario, no OD error

The present analysis is conducted on a perturbed scenario in which SGP4 (Vallado et al., 2006) is used both in the generation of the data set and in the FRED 2.0 algorithm itself. The parameter B^* employed within SGP4 is set to zero, both in the generation and detection of the fragments and in the algorithm. This propagation process involves a conversion from Cartesian coordinates to TEME frame at the initial propagation epoch, followed by a subsequent conversion from the obtained SGP4 elements back to Cartesian coordinates at the final epoch. Within the function which applies this model, these conversions are achieved through a fixed-point iteration loop, thereby introducing an error that accumulates during propagation and could potentially influence the outcomes. The effects of these non negligible errors may appear both in the results of the TCA candidate epochs, as well as in the uncertainty propagation of the covariance matrices, inputs to the PoC evaluation.

In the scenario here presented, no error is introduced in the OD process, and the epoch detection solutions are correct for almost all the 226 fragments that passed through the filters, as reported in Table 7.

Table 7
Perturbed scenario with no OD error. Epoch estimation results. FRED 2.0 correctly detects the event epoch for all simulated fragments except two of them. The estimation for these two outliers falls in the ranking failure case B. This might be attributed to the numerical errors introduced by the conversion SGP4 - TEME when exploiting a dynamical model with the addition of perturbations.

Correct solutions	Computation fails	Ranking fails (A)	Ranking fails (B)
99.1 %	0.0 %	0.0 %	0.9 %

Table 8
Perturbed scenario with no OD error. Median time error percentiles. The epoch estimation is not correctly estimated for all simulated fragments, but for most of them, as confirmed by the 100th percentile, which falls above the three minutes limit. For all other fragments in the data set the epoch estimation is correct and also accurate, as the percentiles from the 5th to the 75th deviate from the true epoch by less than one second.

Percentiles [min]				
5th	25th	50th	75th	100th
9.013e-04	0.003	0.007	0.013	94.268

Table 9
Perturbed scenario with no OD error. Results of the fragment-parent association process. The percentages of true positives and false negatives represent the number of simulated fragments that are correctly or incorrectly associated with the fragmentation event, respectively. Similarly, the percentages of true negatives and false positives correspond to the proportion of objects, which passed the catalogue screening, that are correctly or incorrectly identified as unrelated to the fragmentation event, respectively. In this scenario, the association algorithm performance degrades with respect to the unperturbed case, not being able to associate all the simulated fragments. On the contrary, when tested against false positives, the association algorithm fully succeeds in discarding all objects derived from the catalogue screening and not related to the event.

True positives	False negatives	True negatives	False positives
76.6 %	23.4 %	100.0 %	0.0 %

The median error is reported in terms of percentiles over the simulated fragments in Table 8. A discrepancy in the order of magnitude of the time errors is evident when compared with Table 4. The latter is larger compared to the Keplerian case, which may be attributed to the numerical errors introduced by the conversion SGP4 - TEME, that alter the results of the computation, since neither noise nor error in the state is introduced in the OD process, nor any additional propagation mismatching.

The performance of the association process described in Section 2.1.3 is verified for this scenario as well. In this case, a lower number of fragments than in Section 3.3.1 correctly associate to the event, as observed in Table 9 with respect to the results in Table 5. The performance of the association algorithm is found to be degraded in comparison, as evidenced by its inability to associate all the simulated fragments. Conversely, when evaluated against false positives, the association algorithm fully succeeds in discarding all objects derived from the catalogue screening and not related to the event.

As done in (Montaruli et al., 2023c), an analysis on the Keplerian parameters is conducted, to determine if the reciprocal geometry of parent and fragment orbits can be correlated to the estimation error. It is acknowledged that the MOID computation is inherently less stable when the orientations (hence inclination and RAAN) of the fragment and parent orbits are very close one another. For this reason, significant fluctuations in the MOID values may occur when the fragment orbit is varied from the mean state of one GME to another. Consequently, even when the final solution converges to the right periodicity, the TCA candidate epochs at that periodicity may not centre around the actual fragmentation epoch, but can be distributed around epochs that are several minutes away. This is due to oscillation in the evaluation of the epochs of passage through the MOID.

Additionally, the semi-major axis is expected to influence the outcomes, as the orbital periods are more similar between objects with similar semi-major axes. This suggests that, given a single combination of parent and fragment mean states of the mixtures, their relative distance from one set of TCAs to the one of other periodicities remains relatively unchanged. Since such relative distance enters the computation of the collision probability, the Vittaldev PoC values may not vary largely from one set of TCAs to another one. Consequently, any error or positional uncertainty can lead to an erroneous ranking of the TCAs based on the PoC criterion.

The differences between parent and fragment orbital elements computed at the estimated epoch (for the whole analyzed data set) are reported in Fig. 7, versus the median time error. It can be noticed that significant errors associated with convergence to periodicities other than the third one (ranking fails) tend to arise when the parent and the fragment have similar semi-major axis, which induces a ranking fail (in this case, "Ranking fails (B)"). This finding aligns with the previously mentioned observations concerning the mutual geometry of the two orbits and their correlation with the estimation accuracy. However, no cases related to "Ranking fails (A)" are observed, as evidenced by the percentages in Table 7. On the other hand, errors classified as "Computation fails" also do not occur, so no consideration can be done in this case on the mutual orientation of the two orbits.

For the 226 fragments that were not discarded, this simulation required a computational time of about 3.4 h. This results in approximately 54 s per fragment. A comparison in terms of computational time with the original version of FRED is reported for this scenario as well, in Table 10. Furthermore, the results for both methods are reported in terms of epoch estimation. FRED 2.0 achieves again a higher number of correct epochs detection. This improvement can be attributed to the same considerations in the data set generation as above. Most importantly, the computational effort is reduced significantly. This is likely due to having replaced a MC analysis for representing uncertainties with the use of GMM. However, it is clear that the time required for FRED 2.0 to conduct the simulation of this scenario is higher than the one reported in 6, since SGP4 (Vallado et al., 2006) is more demanding with respect to a Keplerian analytical propagation.

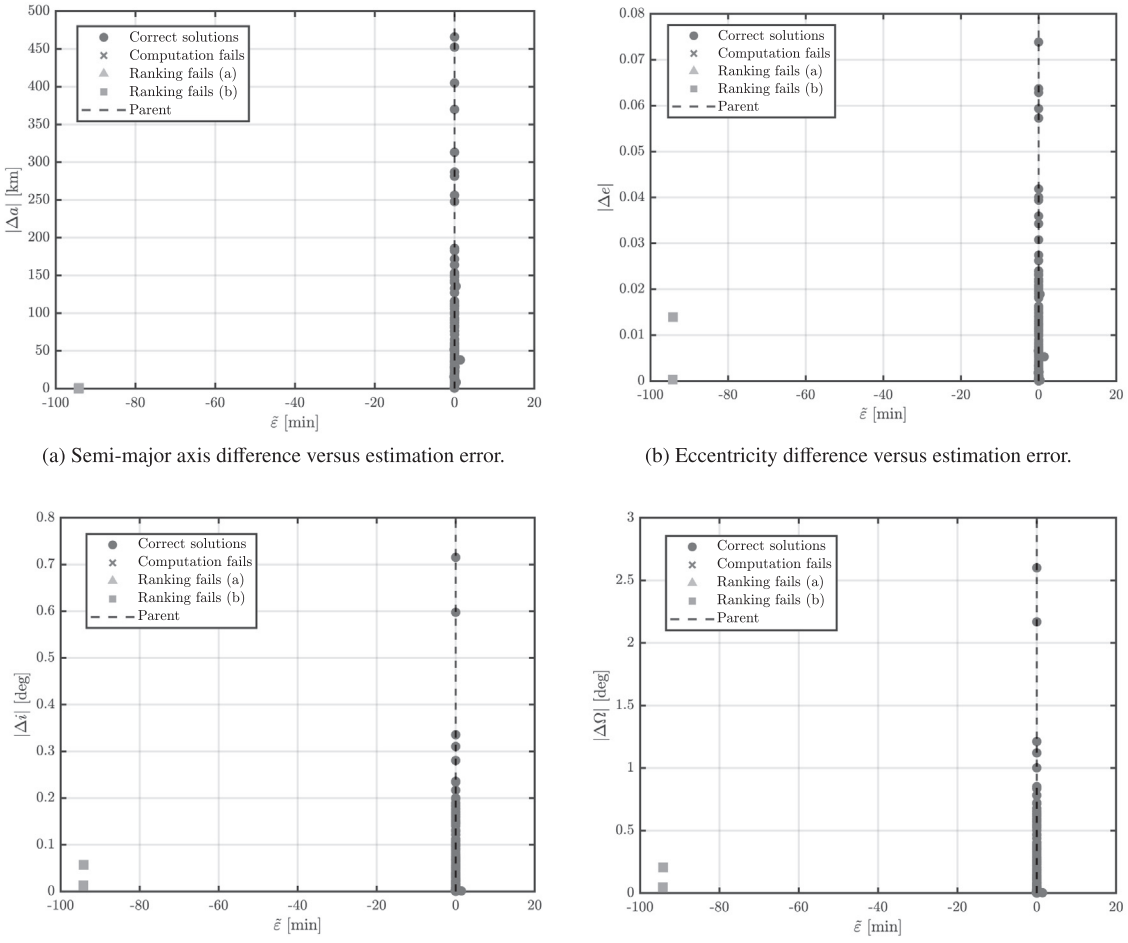

(a) Semi-major axis difference versus estimation error.

(b) Eccentricity difference versus estimation error.

(c) Inclination difference versus estimation error.

(d) RAAN difference versus estimation error.

Fig. 7. Perturbed scenario with no OD error. Difference between Keplerian elements of the parent and fragment objects versus median time error. In this scenario, significant ranking errors (ranking fails of type B) occur when the parent and fragment share similar semi-major axes, as can be seen in Fig. 9a where the two dots superimpose. This confirms the impact of orbital shape on epoch estimation accuracy. No cases of ranking fails type A or computation fails are observed, preventing further analysis on orbital orientation.

Table 10
Perturbed scenario with no OD error. Comparison with FRED in terms of correct solutions in the epoch estimation and computational time per simulation. Source: (Montaruli et al., 2023c). It can be seen that FRED 2.0 achieves a higher percentage of correct solutions with respect to original FRED, by also reducing the computational burden required for the analysis on a single fragment.

	FRED	FRED 2.0
Correct solutions	90.0 %	99.1 %
Computational time per fragment	5 min	54 s

3.3.3. Perturbed scenario, nominal OD error

In order to evaluate the performance of FRED 2.0 tool in a realistic scenario, both orbital perturbations and OD errors are included in the simulation. The detection of the fragments is conducted through the approach described in Section 3.1.5, employing the SGP4 model (Vallado et al., 2006) for the input generation, the OD process and the execution of FRED 2.0 algorithm.

The corresponding results are reported in Table 11.

Table 11
Perturbed scenario, nominal OD error. Epoch estimation results. FRED 2.0 correctly detects the event epoch for almost all the simulated fragments. There are few failures solely due to an unstable estimation of the candidate TCAs (i.e., "Computation fails"). Most incorrect results are attributed to a failure of the PoC-based ranking in selecting the correct periodicity, however only in the "Ranking fails (B)" case. In any case, the results get worse with respect to the scenario lacking of orbit determination errors, due to the difference of the fragments orbital states with respect to the ground truth.

Correct solutions	Computation fails	Ranking fails (A)	Ranking fails (B)
91.6 %	0.4 %	0.0 %	8.0 %

Table 12
Perturbed scenario, nominal OD error. Median time error percentiles. The epoch estimation is not correctly estimated for all simulated fragments, but for most of them, as confirmed by the 100th percentile, which falls above the three minutes limit. In particular, the value corresponding to the 100th percentile indicates the convergence to the most distant periodicity with respect to the correct one. For all other fragments in the data set the epoch estimation is correct and also accurate, as the percentiles from the 5th to the 50th deviate from the true epoch by less than one minute.

Percentiles [min]				
5th	25th	50th	75th	100th
0.014	0.077	0.225	1.224	190.239

As shown in Table 11, the results deteriorate with respect to the case with no errors introduced in the OD (Table 7), due to the difference of the fragments orbital states with respect to the ground truth. It is also interesting to notice from results in Table 11 that there are few failures solely due to an unstable estimation of the candidate TCAs (i.e., "Computation fails"). Most erroneous results are therefore due to a failure of the PoC-based ranking to select the correct periodicity, however only in the "Ranking fails (B)" case. The median error values are shown in terms of percentiles over the simulated fragments in Table 12.

The results of the fragment-parent association are slightly affected by the error in the mean orbital state of the fragments, since the computation of the parameter P^{c}_{tot} is underestimated in one case. Indeed, not all, but almost all simulated fragments are correctly associated to the parent object, as shown clearly in Table 13. Instead, the entire population of "false" fragments derived by catalogue screening is correctly identified and discarded. In general, the results of the association process in this scenario are better than those in Table 9, possibly due to the interaction between the errors due to the OD process and those introduced in SGP4 propagation, which may counteract each other.

Overall, in this scenario, FRED 2.0 method allows to fully characterize the fragmentation event, both in terms of detection of the epoch and in the identification of the associated fragments.

Table 13
Perturbed scenario, nominal OD error. Results of the fragment-parent association process. The percentages of true positives and false negatives represent the number of simulated fragments that are correctly or incorrectly associated with the fragmentation event, respectively. Similarly, the percentages of true negatives and false positives correspond to the proportion of objects, which passed the catalogue screening, that are correctly or incorrectly identified as unrelated to the fragmentation event, respectively. In this scenario, the association is confirmed for almost all the simulated fragments, with the exception of one. Instead, when tested against false positives, the association algorithm fully succeeds in discarding all objects derived from the catalogue screening and not related to the event. Hence, the association process is quite robust to errors introduced in the orbit determination.

True positives	False negatives	True negatives	False positives
99.6 %	0.4 %	100 %	0.0 %

The differences between parent and fragment orbital elements are again reported versus the median time error in absolute value in Fig. 8. It can be noticed again that errors produced by an evident convergence to an erroneous periodicity ("Ranking fails (B)") occur at small differences between the dimensions of parent and fragment semi-major axis (Fig. 8a), and occasionally for similar eccentricities as well. On the other hand, when the two orbits have notably similar orientations (Fig. 8c and 8d), the candidate TCAs can be inaccurately computed. Consequently, the estimated epoch may deviate by a few minutes from the actual epoch, owing to the MOID calculation instability, and so to the "Computation fails", despite being located within the correct periodicity (see cross symbol in Fig. 8). This analysis underscores the conclusion that the failure cases are closely related to the mutual geometry of the orbits. Furthermore, it is evident that the failure cases categorized as "Ranking fails (A)" are not present in the results.

For the 226 fragments, this simulation required a computational time of about 3.5 h, similarly of course to the time required in scenario described in Section 3.3.2. This results in approximately 55.8 s per fragment, that is similar to the time reported in Table 10 for the perturbed scenario, with no OD error. Therefore, introducing an error in the OD process does not induce differences in the computational effort required by FRED 2.0. A comparison in terms of computational time with FRED tool is reported for this scenario as well in Table 14. Also, the results for both methods are reported in terms of epoch estimation. FRED 2.0 achieves a higher number of correct epochs detection also for this scenario. This improvement is related to the same considerations as above. The computational time required for each simulated fragment is again reduced significantly, owing to the use of GMM for the uncertainty representation.

3.4. Sensitivity analysis

Sensitivity analyses are conducted on the perturbed scenario with OD error, to test the robustness of the algorithm to different conditions. Those that may worsen the results are reported below.

- The time elapsed between t_0 and t_{od}: a longer time window in the analysis is expected to amplify the effects of the sources of error with respect to the ground truth.
- The measurements noise: the larger the measurements noise, the larger both the expected orbital state errors and uncertainties resulting from the OD.
- The inaccuracy of the parent ephemeris: the larger the inaccuracy with respect to the ground truth, the larger the error on the mean state in input to the algorithm.
- The discrepancy of the B* parameter: the effects of variable drag can be a major factor for small debris.

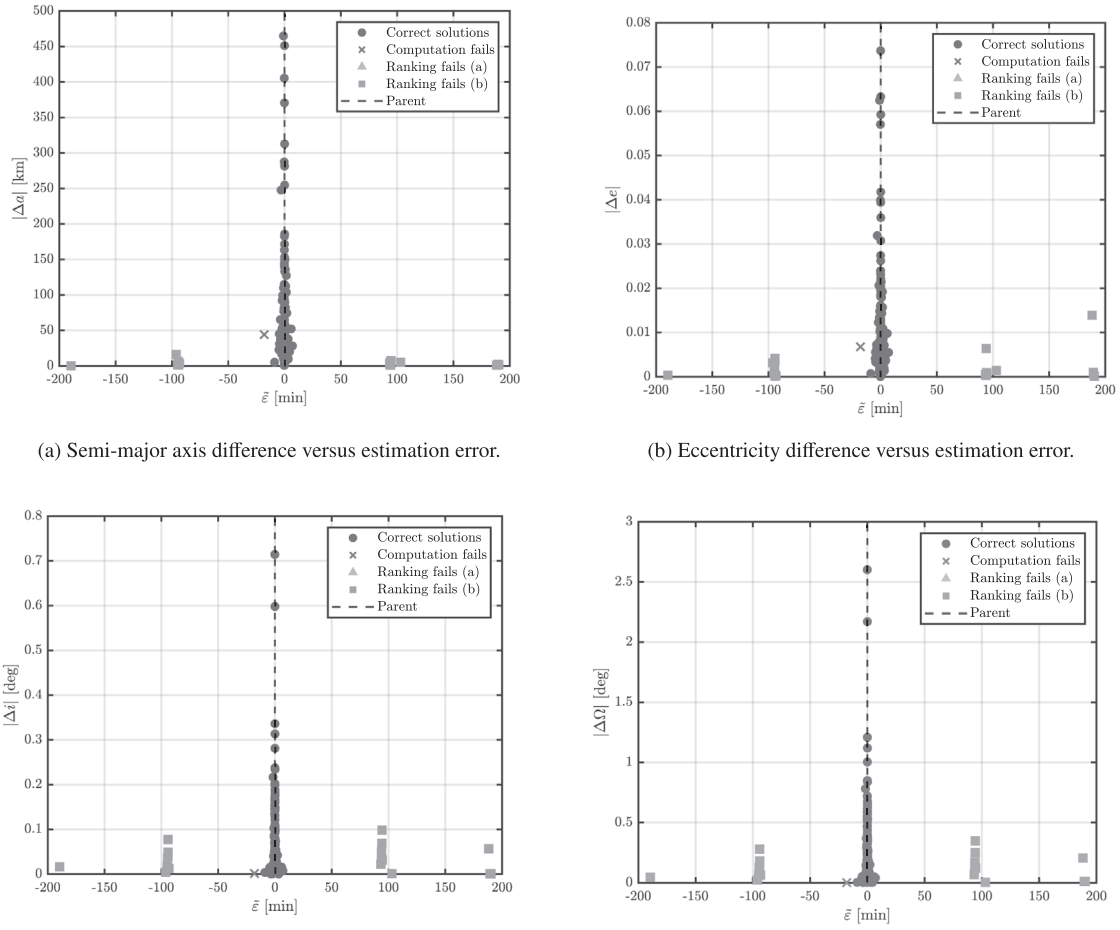

(a) Semi-major axis difference versus estimation error.

(b) Eccentricity difference versus estimation error.

(c) Inclination difference versus estimation error.

(d) RAAN difference versus estimation error.

Fig. 8. Perturbed scenario, nominal OD error. Difference between Keplerian elements of the parent and fragment objects versus median time error. In this scenario, ranking fails of type B occur when the parent and fragment have similar semi-major axes (a) and occasionally eccentricities (b). Additionally, significant orbit orientation similarity contributes to the computation fails (c,d), leading to deviations in the epoch estimation despite correct periodicity convergence (cross symbol). No ranking fails of type A are observed..

Table 14
Perturbed scenario, nominal OD error. Comparison with FRED. Source: (Montaruli et al., 2023c). It can be seen that FRED 2.0 achieves a higher percentage of correct solutions with respect to original FRED, by also reducing the computational burden required for the analysis on a single fragment.

	FRED	FRED 2.0
Correct solutions	68.9 %	91.6 %
Computational time per fragment	5 min	55.8 s

An additional analysis is conducted in order to take into account the potential instance of an ill-conditioned matrix associated to the fragment objects.

3.4.1. OD epoch

In the simulations reported in Section 3.3, the detection of the fragments t_{od} is set to occur 13 h after t_0. In the context of operational procedures, it is possible that the initial detection and OD process may occur at a later time. To test

Table 15
Perturbed scenario with nominal OD error. Sensitivity analysis on the OD epoch versus nominal OD epoch results (in the first line). FRED 2.0 correctly detects the event epoch for most of the simulated fragments, for each OD epoch. However, the more t_{od} is shifted from t_0, the lower becomes the number of fragments leading to a successful solution, due to the amplification of the orbital errors along the propagation window.

Time from t_0	Correct solutions	Computation fails	Ranking fails (A)	Ranking fails (B)
+13 h	91.6 %	0.4 %	0.0 %	8.0 %
+24 h	77.9 %	0.9 %	0.9 %	20.3 %
+48 h	56.4 %	3.6 %	0.9 %	39.1 %

Table 16
Perturbed scenario, nominal OD error and variable OD epoch. Results of the fragment-parent association process. The percentages of true positives and false negatives represent the number of simulated fragments that are correctly or incorrectly associated with the fragmentation event, respectively. Similarly, the percentages of true negatives and false positives correspond to the proportion of objects, which passed the catalogue screening, that are correctly or incorrectly identified as unrelated to the fragmentation event, respectively. In this scenario, the association is confirmed for almost all simulated fragments, however the percentages of correctly associated ones are reduced when the OD epoch is shifted from the nominal case (first line). Similarly, when tested against false positives, the association algorithm succeeds in discarding most of the unrelated catalogued objects, but the number of missed false positives increases the more the OD epoch is shifted from the nominal one (first line).

Time from t_0	True positives	False negatives	True negatives	False positives
+13 h	99.6 %	0.4 %	100 %	0.0 %
+24 h	98.2 %	1.8 %	97.7 %	2.3 %
+48 h	90.2 %	9.8 %	92.1 %	7.9 %

Table 17
Perturbed scenario with nominal OD epoch. Sensitivity analysis on the OD angular measurements noise versus nominal angular noise results (in the first line). FRED 2.0 correctly detects the event epoch for most of the simulated fragments, for each angular measurements noise level. However, as the noise associated with the angular track increases with respect to the nominal case (0.01°), the percentage of failures rises. By increasing the angular noise, no progressive trend is observed in terms of failures either; instead, the results exhibit a non monotonic behavior.

Angular noise	Correct solutions	Computation fails	Ranking fails (A)	Ranking fails (B)
0.01°	91.6 %	0.4 %	0.0 %	8.0 %
0.02°	86.7 %	0.0 %	0.5 %	12.8 %
0.05°	69.5 %	1.3 %	0.0 %	29.2 %
0.1°	79.0 %	0.5 %	0.0 %	20.5 %

this possibility, two shifts of t_{od} are investigated: 24 h and 48 h after the event.

The results for FRED 2.0 epoch detection are reported in Table 15. It can be noticed that the more t_{od} is deviated from t_0, the lower becomes the number of fragments leading to a successful solution. As previously mentioned indeed, the longer the analysis time window, the more both the uncertainties and orbital errors are amplified throughout the propagation. The OD epoch shifting affects the computational time as well, which increases slightly with respect to the nominal case, up to 58 s per fragment, due to a longer propagation window.

The fragment-to-parent association process is also affected by the increase of elapsed time, as clearly visible in Table 16. Delaying the OD epoch, the percentage of simulations achieving correctly the association to the parent object decreases. Specifically, in the + 24 h case, the percentage of simulations correctly associating the fragment to the event is reduced from 99.6 % (OD epoch 13 h after the event) to 98.2 %. This percentage is reduced significantly, to the 90.2 %, in the + 48 h scenario. In any case, the fragment-to-parent association algorithm is able to detect most of the objects related to the event, as well as discarding the ”negatives”. In the latter case however the

Table 18
Perturbed scenario, nominal OD epoch and variable OD error. Results of the fragment-to-parent association process. The percentages of true positives and false negatives represent the number of simulated fragments that are correctly or incorrectly associated with the fragmentation event, respectively. Similarly, the percentages of true negatives and false positives correspond to the proportion of objects, which passed the catalogue screening, that are correctly or incorrectly identified as unrelated to the fragmentation event, respectively. In this scenario, the association is confirmed for almost all simulated fragments; however the percentages of correctly associated ones are reduced when the angular noise introduced in the orbit determination process is increased up to 0.05° and more, with respect to the nominal case (first line). Similarly, when tested against false positives, the association algorithm succeeds in discarding most of the unrelated catalogued objects, but the number of missed false positives increases when the angular noise is increased from the nominal one (first line). However, looking at the increase of angular noise in the non-nominal cases, no linear trend can be identified in the performance degradation of the association process.

Angular noise	True positives	False negatives	True negatives	False positives
0.01°	99.6 %	0.4 %	100 %	0.0 %
0.02°	99.6 %	0.4 %	95.7 %	4.3 %
0.05°	96.9 %	3.1 %	92.3 %	7.7 %
0.10°	98.7 %	1.3 %	95.0 %	5.0 %

performance are again slightly worsen with respect to the nominal results reported in the first line of Table 16.

3.4.2. Measurements noise

As evidenced by the results of simulations presented in Section 3.3, the performance of the routine strongly depends on the accuracy of the OD process. This, in turn, is influenced by factors such as the algorithm used for determination, the length of the observation window, the measurement acquisition frequency, and the quality of these measurements. In particular, a higher noise introduced by the sensor leads to larger uncertainties and discrepancies of the mean state with respect to the real one. Consequently, the robustness of the algorithm shall be investigated on a larger set of noise associated to the simulated measurements. Given the tendency of surveillance radars to exhibit low angular accuracy, the noise level for the range is set constant to the nominal value of 30 m. Simultaneously, variations in the angular noise are introduced: from the nominal value of 0.01° to $0.02^\circ, 0.05^\circ$ and 0.1°, as in (Montaruli et al., 2023c).

Results of the epoch detection are reported in Table 17.

One can observe that, as the noise associated with the angular track increases in comparison with the nominal case (first line of Table 17), convergence to the correct solution becomes more challenging and the percentage of failures rises. It is interesting to notice however that in the case of a 0.1° noise, despite it being higher, the routine performs slightly better compared to the case of 0.05° noise. Possibly, it could occur that the number of correct solutions actually improves due to the interaction between the higher OD errors of this scenario and other numerical errors (such as those introduced in the propagation with SGP4), leading to find the highest PoC value in correspondence of the correct candidate epoch. Therefore, by increasing the angular noise, no monotonic trend is observed in terms of failures either.

The association process results are reported in Table 18. Regarding the association of the simulated fragments, the performance here are partially affected. With respect to the almost complete success rate of the nominal case (first line of Table 18, that is of 99.6 %), the situation does not change when increasing the angular noise to 0.02°. Instead, with larger errors, the correct associations degrade to 96.9 % for 0.05° noise and 98.7 % for 0.1° noise. The number of successful associations is still very high, despite many success cases do not lead to a correct estimate of the event epoch (Table 17). By instead looking at the analysis of the "false" fragments (Table 18, columns on the right), most of the unrelated objects are correctly discarded (in the worst case 92.3 %). However, the method is sensitive to higher OD errors, since the number of false associations increases with respect to the nominal case (first line of Table 18), where the entire population of catalogued objects is correctly found to have a P^c_{tot} value that is not compliant with the threshold. Overall, the non monotonic behaviour while increasing the angular noise is confirmed also for the association process.

3.4.3. Parent mean state perturbation

The results presented in all preceding sections have been obtained using a statistical representation of both objects. However, it is important to note that the mean state of the parent object is never altered from the ground truth (represented by the state acquired from the last available TLE before the event), except during the splitting process required for the GMM generation. However, in real case scenarios, the prediction of the parent orbital state is not completely accurate, and inaccuracies shall be taken into account. Therefore, it is relevant to investigate the impact of an inaccurate orbital state of the parent object on the algorithm performance. This perturbation is introduced as follows:

Table 19
Perturbed scenario with nominal OD error and nominal OD epoch. Sensitivity analysis on the parent state perturbation. In the first line, the results of the scenario with nominal OD error, nominal OD epoch and nominal input parent state are reported for comparison. The mismatches on the parent orbital state generally degrade the epoch estimation accuracy, except in a few cases. The association algorithm occasionally outperforms the nominal case but is mostly slightly affected. No clear trend emerges due to complex error interactions. Most failures stem from incorrect periodicity convergence rather than inaccurate TCAs computation.

n°	Correct solutions	Computation fails	Ranking fails (A)	Ranking fails (B)	True positives	ε_r [km]	ε_v [km/s]
-	91.6 %	0.4 %	0.0 %	8.0 %	99.6 %	-	-
1	88.1 %	0.0 %	0.0 %	11.9 %	98.7 %	0.1488	1.58e-04
2	85.4 %	1.3 %	0.0 %	13.3 %	99.1 %	0.1931	2.12e-04
3	90.7 %	0.4 %	0.0 %	8.8 %	100.0 %	0.4757	5.30e-04
4	92.9 %	0.9 %	0.0 %	6.2 %	100.0 %	0.4845	5.38e-04
5	92.0 %	0.9 %	0.0 %	7.1 %	99.1 %	0.5101	5.71e-04
6	92.9 %	0.5 %	0.0 %	6.6 %	100.0 %	0.6335	6.93e-04
7	91.6 %	0.0 %	0.0 %	8.4 %	99.1 %	0.8047	8.85e-04
8	84.5 %	0.9 %	0.4 %	14.2 %	96.0 %	1.2844	0.0014
9	90.3 %	0.9 %	0.0 %	8.8 %	99.1 %	1.6257	0.0018
10	90.3 %	1.3 %	0.0 %	8.4 %	98.2 %	2.8786	0.0032

1. 10,000 random multivariate samples ($\boldsymbol{x}_s^p$) are generated from the parent orbital state, distributed according to the covariance matrix $\boldsymbol{P}^p$.
2. The perturbed samples are ranked according to their statistical distance with respect to the initial distribution ($\{\boldsymbol{x}^p, \boldsymbol{P}^p\}$), by computing the Mahalanobis distance for each sample:

$$d_M(\boldsymbol{x}_s^p) = \sqrt{(\boldsymbol{x}_s^p - \boldsymbol{x}^p)^T (\boldsymbol{P}^p)^{-1} (\boldsymbol{x}_s^p - \boldsymbol{x}^p)}$$

   and by selecting 10 values, going from the lowest to the highest. The 10 corresponding state samples are the only considered from now on.
3. 10 simulations are repeated with FRED 2.0, providing in input as the parent ephemeris each perturbed sample just derived.

The results of the different runs are reported in Table 19, for the scenario with perturbed dynamics and nominal OD epoch and OD error. Each simulation is associated to a different error between the perturbed parent ephemeris and the ground truth. The norm of this error is expressed in terms of position and velocity in the results, respectively as ε_r and ε_v. Additionally, a column expressing the percentage of successful associations between the simulated fragment and the parent is reported.

As can be observed from the results presented in Table 19, the perturbation on the orbital state of the parent object generally leads to a decrease in the number of correct solutions for the epoch estimation, resulting in a degradation of the performance. The exceptions are runs 4, 5, 6 and 7, where the number of correct solutions is slightly higher (or equal) compared to the nominal case results (first line of Table 19). As for the fragment-to-parent association algorithm, it occasionally performs better than in the nominal case, reaching percentages of 100 % of correctly associated objects, against the nominal 99.6 % reported in the first line of Table 19. However in most of the 10 simulations the introduced perturbation slightly degrades the number of true positives found. Therefore, this process as well is compromised by having modified the input TLE state. From these considerations, it appears that a general trend cannot be identified. This is likely due to the combination of errors introduced by the perturbation of the initial parent ephemeris and those caused by the OD error on the fragments detection, and by the conversion from SGP4 elements to Cartesian coordinates and back. These factors may indeed influence and compensate each other in a not linear way that is not entirely quantitatively interpretable. It is evident, on the other hand, that in most failure cases the metric of the highest PoC converges to an incorrect periodicity, with a time error that is not mitigated by its uncertainty, while it occurs less frequently that failures are due exclusively to inaccurate TCAs.

In any case, in this scenario as well, FRED 2.0 achieves the goal of an accurate estimation of the epoch and detection of the fragments for the majority of simulated population.

Table 21
Perturbed scenario with nominal OD error, nominal OD epoch and modified B* value for both parent and fragments objects. Results of the fragment-to-parent association process. The association is confirmed for almost all simulated fragments, however the percentage of correctly associated ones is reduced when the B* values are shifted from the nominal case (first line).

Parent B*	Fragment B*	True positives	False negatives
0	0	99.6 %	0.4 %
0.694e-04	1e-05	87.1 %	12.9 %
0.694e-04	1e-04	86.5 %	13.5 %
0.694e-04	1e-03	87.0 %	13.0 %

3.4.4. Variable B*

In the nominal simulations (Section 3.3.3), the SGP4 propagator employs a ballistic coefficient B* equal to zero, assigned to both the parent object and its fragments, thereby neglecting orbital decay. Given the crucial role of atmospheric drag in circularizing and reducing low Earth orbit semi-major axes, a sensitivity analysis is performed, employing a non-zero B* value for the parent object and for the fragments. Specifically, a value of 0.69413e-04 is assigned to the parent object, while three cases of B* value are considered for all the fragments: 1e-03, 1e-04 and 1e-05. It is worth to remark that the B* value is set each time equal both in the fragments data set generation and inside the algorithm. Therefore, the analysis evaluates the influence of B* perturbations, notably drag, on the stochastic distribution and on the error growth in OD through ampli-

Table 20
Perturbed scenario with nominal OD error, nominal OD epoch and modified B* value for both parent and fragments objects. In all cases with modified B*, FRED 2.0 correctly detects the event epoch for the majority of the simulated fragments. The incorrect estimations fall mostly in the computation failure and ranking fail of type (B). The performance deteriorate in any case with respect to the zero B* used in the nominal scenario (first line), where the drag effect is not included in the SGP4 propagation. This degradation is attributed to the addition of the drag effect in the perturbations.

Parent B*	Fragments B*	Correct solutions	Computation fails	Ranking fails (A)	Ranking fails (B)
0	0	91.6 %	0.4 %	0.0 %	8.0 %
0.694e-04	1e-05	73.3 %	12.0 %	0.4 %	14.3 %
0.694e-04	1e-04	80.4 %	6.5 %	0.0 %	13.1 %
0.694e-04	1e-03	73.1 %	12.5 %	0.0 %	14.4 %

Table 22
Unperturbed scenario with no OD error, nominal OD epoch and modified covariance matrix for fragments objects. FRED 2.0 epoch detection is significantly impacted by an ill and large covariance matrix. The majority of simulated fragments are unable to identify the correct periodicity due to the dilution effect arising. Conversely, in scenarios where the uncertainties are negligible, as illustrated in the first line, the epoch is consistently and accurately identified.

Covariance matrix	Correct solutions	Computation fails	Ranking fails (A)	Ranking fails (B)
$\boldsymbol{P}^p$	100 %	0 %	0 %	0 %
$\boldsymbol{P}^p \times 1e+04$	6.5 %	0.0 %	10.1 %	83.4 %

fication effects, neglecting the mismatching between the B* in data set generation (ground-truth) and the B* in the algorithm. This phenomenon arises because a non-zero B* in the OD process amplifies the variations in the mean states of the mixtures. Furthermore, the selection of three different B* values for the fragments facilitates the analysis of the impact of altering the ballistic coefficient and, consequently, the variable drag perturbation on the performance of the algorithm on small objects, such as fragments. The execution of FRED 2.0 in the scenario involving nominal OD error and perturbations (see Section 3.1.5), with the modification of the B* only, results in the outcomes here presented. The epoch detection solutions are reported in Table 20 for the 225 fragments that passed through the filters.

As shown in Table 20, the results deteriorate with respect to the case with negligible drag perturbation (first line). In all the cases, most erroneous results are due to a failure of the PoC-based ranking to select the correct periodicity, in the "Ranking fails (B)" case. When the fragments B* value is increased (B* = 1e-03) the effect of drag is larger, and this is reflected in the percentage of correct solutions, which is more degraded than in the other cases.

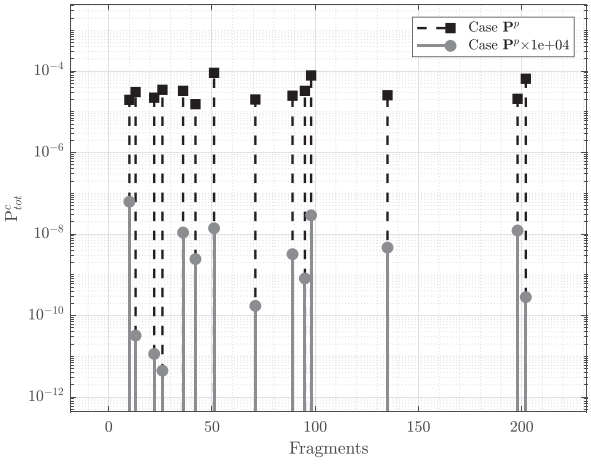

Fig. 9. Unperturbed scenario with no OD error, nominal OD epoch. Original and modified covariance matrix of fragments objects. Values of total probability in time P^c_{tot}, for fragments with correct periodicity detection, according to the results of the modified covariance case (logarithmic scale). The PoC values decrease significantly (grey stems) due to the dilution effect caused by the large and ill initial uncertainty, with respect to the unmodified and small covariance case (black stems).

The results of the fragment-to-parent association are affected as well by the addition of the drag contribution in the dynamics. Not all, but almost all simulated fragments are correctly associated to the parent object, as shown in Table 21. The number of correct associations is degraded with respect to the nominal scenario results (first line), for all the variations of the fragments B*. In a manner analogous to the epoch detection results, the fragment-to-parent association is found to be more negatively impacted with growing B* values (even if not linearly), as a greater number of associations are missed due to the growing effect of the drag perturbation.

3.4.5. Ill-conditioned covariance

In the immediate aftermath of a break-up event, there may be a high variation of the initial covariance matrices (which may be very large), particularly in the case of relevantly eccentric fragments. In such cases, the probability of collision, used as a metric in the algorithm, may be subjected to dilution and therefore affect the performance of the method. It is important then to take into consideration the presence of such debris pieces following high-energy events. The present additional analysis is, accordingly, reported herein to take into account this aspect. Specifically, the simulation is conducted through FRED 2.0 in the scenario involving no OD errors (see Section 3.1.5) and and an unperturbed dynamics. Subsequent to the retrieval of the mean estimated orbital states of the fragment objects, their associated covariance matrix is fixed to an ill-conditioned and very high one. This covariance is obtained by multiplying the matrix in Eq. 7 by a factor of 1e + 04, resulting in excessively amplified position and velocity uncertainties (σ_r = 87.6 km and σ_v = 0.1 km/s). Additionally, the same matrix is ill-conditioned, having a condition number of 2.9e + 23. This situation of increased uncertainty and, consequently, dilution on the computation of the total collision probability, is expected to affect the results of the algorithm. As expected, a high failure rate is observed in the epoch detection method (Table 22), as well as a drop of certain P^c_{tot} values resulting from the influence of a diluted uncertainty (Fig. 9). This outcome is further supported by the comparison with the unperturbed scenario with no OD errors (Section 3.3.1), where the epoch detection is accurately achieved (first line of Table 22). In this condition, the total PoC employed for the association (black stems in Fig. 9) is only marginally

influenced by dilution, which arises solely from the perturbation of the mixture components mean states with respect to the true mean state. It is worth to remark that the P^c_{tot} values in Fig. 9 only refer to those fragments which yeld a correct detection of at least the event periodicity, through the PoC metric, under the case of employing the large ill-conditioned covariance matrix.

4. Operational scenario

The performance of FRED 2.0 tool is also assessed on real data, in order to verify its application to a real operational scenario. Specifically, Section 4.1 describes the real break-up event used as the real test case, along with the associated information. The results of this test case, with respect to the fragment association and event epoch computation algorithms, are presented in Section 4.2.

4.1. Real test case

The real case tested and described in this section is the fragmentation of the LEO object CZ-6A R/B, identified as the explosion of a Chinese launcher upper stage, occurred on November 12, 2022.

The data used to perform FRED 2.0 execution include for the fragment objects a set of 433 TLEs derived from the data acquired after the event by the Space Situational Awareness Centre (C-SSA) of the Italian Air Force, which manages the fragmentation analysis service of the EUSST consortium. Since no information on the uncertainty was associated to these orbital states, for the fragment objects a fixed covariance matrix (with standard deviations on position and velocity of respectively 0.0262 km and $7.02e-04$ km/s) is associated to all of them. The parent object ephemeris, used as input, is derived from a TLE present on Space-Track (Space-Track, 2023) and dated to few hours before the event, that was guessed to have taken place on November 12th, 2022, between 05:24 and 05:29 UTC (Montaruli et al., 2023a). The orbital parameters related to the parent object TLE used in the following analysis are reported in Table 23. The covariance matrix associated to the stochastic TLE information of the parent is derived by applying the approach described in Section 2.2, to a set of 5 TLEs related to the parent object NORAD ID and available on Space-Track (Space-Track, 2023). These TLEs are dated after the event, up to 18:03:50 UTC of November 12th, 2022. The resulting covariance matrix is reported in Eq. 11, with elements referred to uncertainties expressed in km and km/s.

Table 23
CZ-6A R/B Keplerian elements at t_{eph}: 2022–11-12 03:24:14.5639 UTC.

a [km]	e [-]	i [deg]	Ω [deg]	ω [deg]	M [deg]	B*
7214.4	0.0028	98.725	320.896	10.263	0	0

$$\boldsymbol{P}^p = \begin{bmatrix} 5.8129 & -2.6805 & 44.4553 & -0.0267 & 0.0308 & -0.0048 \\ -2.6805 & 1.2363 & -20.5009 & 0.0123 & -0.0142 & 0.0022 \\ 44.4553 & -20.5009 & 340.0024 & -0.2041 & 0.2358 & -0.0365 \\ -0.0267 & 0.0123 & -0.2041 & 0.0001 & -0.0001 & 0.00002 \\ 0.0308 & -0.0142 & 0.2358 & -0.0001 & 0.0002 & -0.00003 \\ -0.0048 & 0.0022 & -0.0365 & 0.00002 & -0.00003 & 0.000004 \end{bmatrix} \tag{11}$$

It is evident from Eq. 11 that the parent covariance is greater than that of the fragments. This can be attributed to the TLEs of the parent object employed in the method described in Section 2.2. These TLEs exhibit a lower degree of consistency with one another, consequently resulting in a covariance matrix characterised by elevated uncertainties in comparison to that of the fragments. The fixed covariance of the latter, above mentioned, is instead obtained from a fictitious however realistic OD result.

4.2. Real data analysis

FRED 2.0 is then run to search for the fragmentation epoch of the event and the associated objects, in an analysis time window ranging from the last available ephemeris epoch up to the 08:00:00 UTC on 12 November. The number of GMEs used for the parent and fragment objects uncertainty representation is set to $N_p = N_f = 9$. The parent HBR, used as the combined HBR for the collision probability computation, is fixed to 3 m, according to available information on the upper stage dimensions of Long March launcher (Krebs, 2025). The threshold on the lower bound of P^c_{tot} to detect a positive fragment-parent association, described in Section 2.1.3, is set equal to 10^{-10}. Finally, the model exploited for the propagation of the orbital states and uncertainties in the UT is SGP4 (Vallado et al., 2006).

Differently from the simulated framework in Section 3, the aim here is to replicate an operational scenario similar to what may occur following a fragmentation event alert. For this reason, first, the entire set of real data of the input fragments is examined by FRED 2.0 epoch detection algorithm, until the computation of the TCA epochs clusters. The total collision probabilities over time are subsequently calculated in the fragment-to-parent association algorithm, and the fragments that are found to be associated to the event (as the value of P^c_{tot} satisfies the set threshold) are retained in the data set, while the rest are not considered. It is important to emphasise that this process is applied to one fragment of the initial data set at a time, compared with the same TLE of the parent object reported in Table 23. For the associated and retained fragment objects, the epoch detection algorithm is then completed with the PoC-based ranking metric, and the estimated event epoch is computed for each of them. Thus, the epoch estimation results reported below refer to the set of fragments that are initially confirmed by the association process, and for which the computations are completed by the end of the epoch detection algorithm.

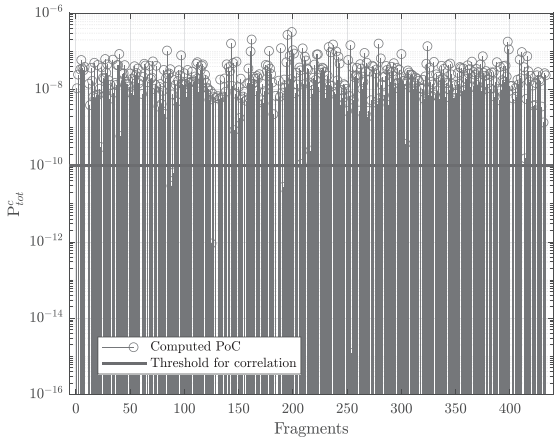

(a) Values of total probability in time P^c_{tot} for each fragment (logarithmic scale), versus lower-bound threshold to confirm the fragment-to-parent association.

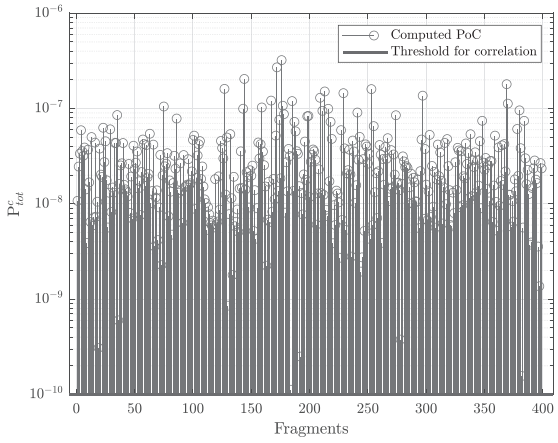

(b) Values of total probability in time P^c_{tot} for each associated fragment (logarithmic scale), versus lower-bound threshold to confirm the fragment-to-parent association.

Fig. 10. Perturbed scenario on real data. Results of FRED 2.0 fragment-to-parent associations algorithm, for all fragment objects not discarded by the method filters (a) and only for the fragments confirmed to be related to the event by the association process (b). The majority of simulated fragments are correctly associated to the parent object, while for some of them the association is not confirmed, since the corresponding values of total probability over time P^c_{tot} fall below the threshold set to 10^{-10}, represented by the black line (a). Obviously, for all fragments resulting associated to the parent object, the value of P^c_{tot} overcomes the threshold (b). Only for these the simulation of the epoch detection is executed till the end..

Table 24
Perturbed scenario on real data. Epoch estimation results. FRED 2.0 correctly detects the event epoch along almost all fragments associated to the event. There are few failures solely due to an unstable estimation of the candidate TCAs (i.e., "Computation fails"). Most incorrect results are attributed to a failure of the PoC-based ranking in selecting the correct periodicity, however only in the "Ranking fails (B)" case.

Correct solutions	Computation fails	Ranking fails (A)	Ranking fails (B)
94.2 %	1.0 %	0.0 %	4.8 %

4.2.1. Results

Firstly, 430 fragments are not discarded by the filters on the computed transit epochs through the MOID and on the DCA value related to the refined TCA epochs. The non-discarded fragments, as mentioned above, first undergo the TCA epochs computation and then the fragment-to-parent association process. Of the 430 fragments analysed, 399 show a positive association to the event. This results in a 92.8 % of "True positives" and a 7.2 % of "False negatives". The total probability over time of all the 430 fragment objects that were not discarded by the filters internal to the epoch detection algorithm is reported in Fig. 10a, against the threshold required to confirm the association. On the right, in Fig. 10b, the same is reported only for the associated fragments, obviously noticing that these values always overcome the threshold of 10^{-10}.

As previously stated, the set of associated fragments which shall undergo the complete epoch estimation is comprised of 399 of the initial 433 TLEs. The results of the epoch estimation approach, in terms of percentages above defined, are reported in Table 24. The epoch detection solutions are coherent with the reference one in (Montaruli et al., 2023a) for almost all the 399 associated fragments.

The median error $|\tilde{\varepsilon}|$ is reported for the analysed data set, in absolute value and in minutes, in terms of percentiles (Table 25). These data reflect the presence of the few failures in the epoch estimation reported previously in Table 24. The differences between parent and orbital elements of the fragments associated to the event are reported versus the median time error in absolute value in Fig. 11. It can be noticed that errors caused by an apparent convergence to an incorrect periodicity ("Ranking fails (B)") occur at smaller differences between the dimensions of parent and fragment semi-major axis (Fig. 11a), and occasion-

Table 25
Perturbed scenario on real data. Median time error percentiles. The epoch estimation is not correctly estimated for all simulated fragments, but for most of them, as confirmed by the 100th percentile, which falls above the three minutes limit. For all other fragments in the data set the epoch estimation is correct and also accurate, as the percentiles from the 5th to the 75th deviate from the true epoch by less than three minutes.

Percentiles [min]				
5th	25th	50th	75th	100th
0.215	0.695	0.895	2.121	102.940

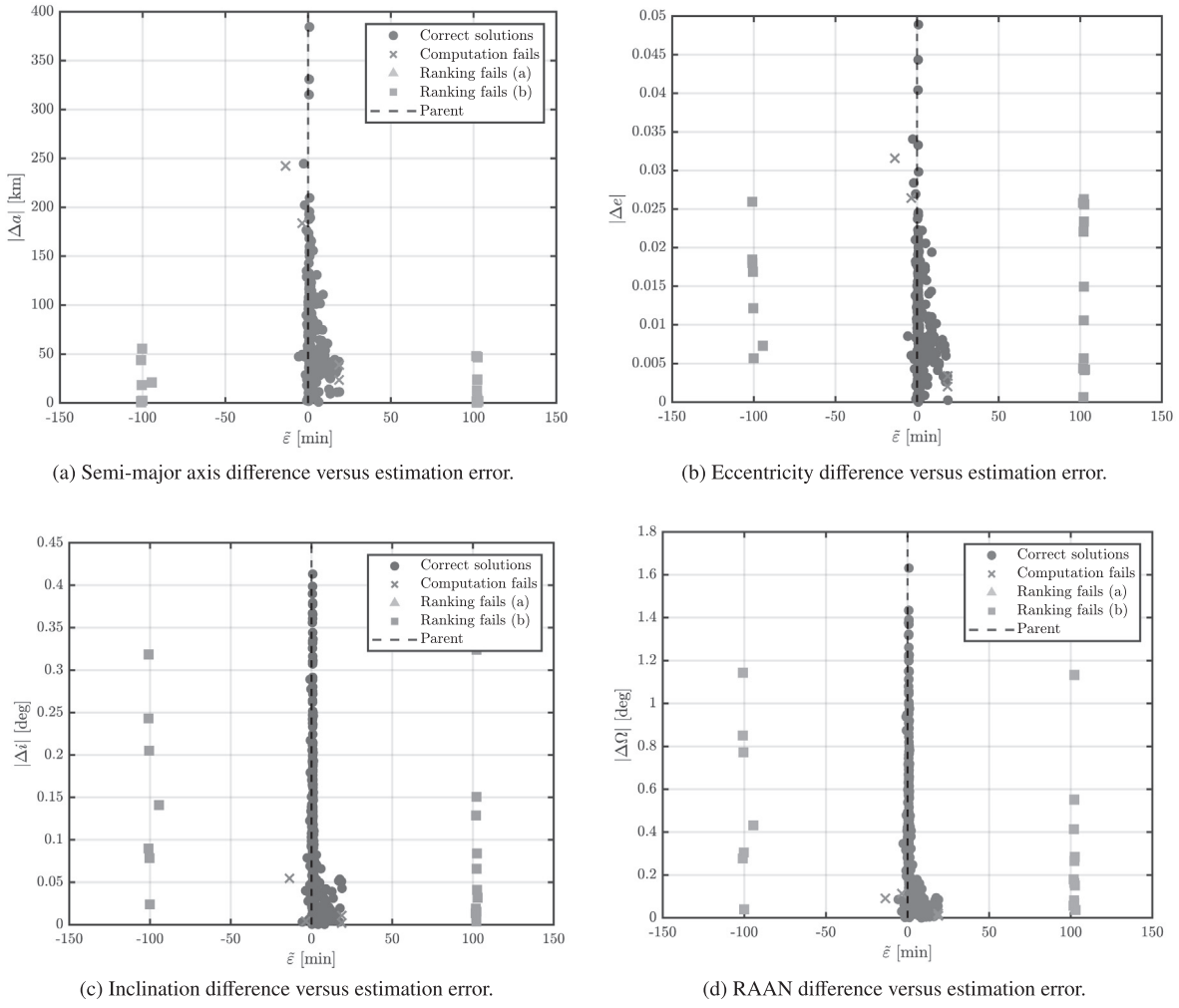

(a) Semi-major axis difference versus estimation error.

(b) Eccentricity difference versus estimation error.

(c) Inclination difference versus estimation error.

(d) RAAN difference versus estimation error.

Fig. 11. Perturbed scenario on real data. Difference between Keplerian elements of the parent and fragment objects versus median time error. In this scenario, ranking fails of type B occur when the parent and fragment have similar semi-major axes (a) and occasionally eccentricities (b). Additionally, significant orbit orientation similarity contributes to the computation fails (c,d), leading to deviations in the epoch estimation despite correct periodicity convergence (cross symbol). No ranking fails of type A are observed..

ally for similar eccentricities as well (Fig. 11b). On the other hand, when the two orbits have quite similar orientations (Fig. 11c and 11d), this becomes a significant factor contributing to inaccuracies in computing the candidate TCAs. As a result, due to the instability of the MOID computation, the estimate may be a few minutes off from the actual epoch, leading to the "Computation fails", despite being in the correct periodicity (cross symbol in Fig. 11). This analysis again confirms that the failure cases are closely related to the mutual geometry of the orbits. In addition, the failure cases defined as "Ranking fails (A)" are not present.

5. Conclusions

The research presented in this paper aims to contribute to improving the ability to characterize fragmentation events in the near-Earth environment, within the first few hours after an event alert, in order to mitigate the damage caused by debris production and dispersion. The implemented tool can determine the epoch of a fragmentation event given a single fragment orbital state and one ephemeris of the fragmented object. This is achieved through a stochastic representation and manipulation of both fragment and parent orbital states. In addition, a criterion has been implemented to associate the fragment to the original spacecraft, allowing for a comprehensive event characterization. Both methodologies are stochastic and exploit techniques drawn from the conjunction analysis.

Several important conclusions can be drawn from the simulation results. The tool operates with a 100% success rate under ideal conditions, implying Keplerian propagation and no error introduced into the OD process. In more realistic scenarios, the algorithm generally converges to the correct solution but it is less robust when fragment and parent orbits have similar orientations or shapes. The convergence to a wrong periodicity is identified as the primary cause of failures, even in the presence of orbit determina-

tion errors. A sensitivity analysis reveals that results are degraded as the time between the fragmentation event and the orbit determination increases. Conversely, an increase in measurement noise and a degradation in the representation of the parent orbital state result in oscillatory outcomes. The use of Gaussian Mixture models for uncertainty representation has been demonstrated to enhance the computational efficiency of the algorithm. A real case application of FRED 2.0 algorithm generally confirms the outcome of the numerical analysis.

A first future extension of this work includes testing different propagation models to introduce additional disturbances and customize the dynamics model, as the use of high-fidelity propagators ensures greater realism despite higher computational demands. Another aspect of interest is evaluating the impact of varying the number of GMEs, since finer discretization of the initial Gaussian distribution theoretically improves the mixture fitting under nonlinear propagation. Simulation results also highlight the underestimation of collision probability when increasing the OD uncertainty, affecting therefore the PoC-based ranking metric. Future research may therefore introduce alternative CA methods to address this dilution problem, inspired by the approaches presented in (Alfano, 2005; Miller, 2022; Laporte, 2014; Massey, 1951). Finally, a procedure to characterize the fragmentation event directly in the measurement space of the observed fragment would represent an added value.

Declaration of competing interest

The authors declare that they have no known competing financial interests or personal relationships that could have appeared to influence the work reported in this paper.

Acknowledgments

This research has received funding as part of the work developed for the agreement n. 2023–37-HH.0 for the project "Attività tecnico-scientifiche di supporto a C-SSA/ISOC e simulazione di architetture di sensori per SST", established between the Italian Space Agency (ASI) and Politecnico di Milano (POLIMI).

The authors are grateful to Cap. Damiano Errico, Magg. Giuseppe Pariti and Ten. Col. Claudio Gizzi of the Italian Air Force for their key contribution to the analysis here presented.

References

Alfano, S., 2005. A numerical implementation of spherical object collision probability. J. Astronaut. Sci. 53, 103–109.

Andrişan, R.L., Ioniţă, A.G., González, R.D., et al., 2016. Fragmentation event model and assessment tool (fremat) supporting on-orbit fragmentation analysis. In: 7th European Conference on Space Debris.

Bianchi, G., Mariotti, S., Montaruli, M. et al., 2023. The new transmitting antenna for birales. Mater. Res. Proc., 37, 474–477. URL: https://www.scopus.com/record/display.uri?eid=2-s2.0-85185778349&origin=resultslist. doi:10.21741/9781644902813-104. All Open Access, Hybrid Gold Open Access.

Bonaccorsi, S., Montaruli, M.F., Di Lizia, P. et al., 2024. Conjunction analysis software suite for space surveillance and tracking. Aerospace, 11(2).https://www.mdpi.com/2226-4310/11/2/122. doi:10.3390/aerospace11020122.

Chan, F.K., 2008. Spacecraft collision probability. American Institute of Aeronautics and Astronautics Inc..

Cordelli, E., Vananti, A., Schildknecht, T., 2020. Analysis of laser ranges and angular measurements data fusion for space debris orbit determination. Adv. Space Res. 65 (1), 419–434. https://doi.org/10.1016/j.asr.2019.11.009, URL: https://www.scopus.com/inward/record.uri?eid=2-s2.0-85076231165&doi=10.1016%2fj.asr.2019.11.009&partnerID=40&md5=a85d9f9aef76ae3fb4753673b2713f49.

Dimare, L., Cicalò, S., Rossi, A. et al., 2019. In-orbit fragmentation characterization and parent bodies identification by means of orbital distances. In: First International Orbital Debris Conference (p. 6007). volume 2109.

ESA, 2024a. ESA'S Annual Space Environment Report. Technical Report ESA ESOC Robert-Bosch-Strasse 5 D-64293 Darmstadt Germany.

ESA, 2024b. Space debris by the numbers. Available online at: https://www.esa.int/Space_Safety/Space_Debris/Space_debris_by_the_numbers. Last accessed: 2024-09-13.

Ester, M., Kriegel, H.-P., Sander, J., et al., 1996. A density-based algorithm for discovering clusters in large spatial databases with noise. In kdd volume 96, 226–231.

EUSST, 2023a. Eu space surveillance and tracking: About us. Available online at.

EUSST, 2023b. Eu space surveillance and tracking: Services. Available online at.

Giudici, L., Colombo, C., Horstmann, A., et al., 2024. Density-based evolutionary model of the space debris environment in low-earth orbit. Acta Astronaut. 219, 115–127.

Gronchi, G.F., 2002. On the stationary points of the squared distance between two ellipses with a common focus. SIAM J. Scient. Comput. 24 (1), 61–80. https://doi.org/10.1137/S1064827500374170.

Huber, P., 2004. Robust Statistics. Wiley Series in Probability and Statistics - Applied Probability and Statistics Section Series. Wiley. URL: https://books.google.it/books?id=e62RhdqIdMkC.

IADC, 2021. Space debris mitigation guidelines. Inter-Agency Space Debris Coordination Committee.

Johnson, N.L., Krisko, P.H., Liou, J.-C., et al., 2001. Nasa's new breakup model of evolve 4.0. Adv. Space Res. 28 (9), 1377–1384.

Julier, S., Uhlmann, J., Durrant-Whyte, H.F., 2000. A new method for the nonlinear transformation of means and covariances in filters and estimators. IEEE Trans. Automatic Control 45 (3), 477–482.

Kessler, D.J., Cour-Palais, B.G., 1978. Collision frequency of artificial satellites: the creation of a debris belt. J. Geophys. Res.: Space Phys. 83 (A6), 2637–2646.

Krebs, G.D., 2025. Cz-6a (chang zheng-6a). URL: https://space.skyrocket.de/doc_lau_det/cz-6a.htm gunter's Space Page. Accessed: January 26, 2025.

Laporte, F., 2014. Jac software, solving conjunction assessment issues. In: Advanced Maui Optical and Space Surveillance Technologies Conference, p. E4.

LeoLabs, 2021. Analysis of the cosmos 1408 breakup. URL: https://leolabs-space.medium.com/analysis-of-the-cosmos-1408-breakup-71b32de5641f.

Letizia, F., Colombo, C., Lewis, H.G., 2015. Analytical model for the propagation of small-debris-object clouds after fragmentations. J. Guid., Control, Dynam. 38 (8), 1478–1491.

Mains, D., Peterson, G., McVey, J., et al., 2024. Forensic analysis of recent debris-generating events. Journal of Space Safety Engineering. https://doi.org/10.1016/j.jsse.2024.06.006, URL: https://www.sciencedirect.com/science/article/pii/S2468896724001010.

Maruskin, J.M., Scheeres, D.J., Alfriend, K.T., 2009. Correlation of optical observations of objects in earth orbit. J. Guid., Control, Dynam. 32 (1), 194–209.

Massey Jr, F.J., 1951. The kolmogorov-smirnov test for goodness of fit. Journal of the American statistical Association 46 (253), 68–78.
MathWorks, 2023. Matlab version: 9.14.0 (r2023a). URL: https://www.-mathworks.com the MathWorks Inc.
Matney, M., 2000. An introduction to the satellite breakup risk assesment model (sbram).
Matney, M.J., Theall, J.R., McKay, G.A., 1999. The use of the satellite breakup risk assessment model (sbram) to characterize collision risk to manned spacecraft. International Astronautical Congress IAA-99-IAA. 6 (5), 09.
Miller, C., 2022. Efforts in Solving the Dilution Problem for Orbital Collisions. Master's thesis Purdue University.
Montaruli, M., Di Lizia, P., Tebaldini, S. et al., 2024a. Adaptive track approach for multiple sources scenarios during radar survey for space surveillance applications. Aerospace Sci. Technol., (p. 109307). https://www.sciencedirect.com/science/article/pii/S1270963824004383. doi: 10.1016/j.ast.2024.109307.
Montaruli, M.F., Bonaccorsi, S., Muciaccia, A. et al., 2023a. Assessment of the cz-6a r/b and the h-2a deb fragmentation events. In: Aerospace Europe Conference 2023-Joint 10th EUCASS-9th CEAS Conference (pp. 1–10).
Montaruli, M.F., De Luca, M.A., Massari, M. et al., 2024b. Operational angular track reconstruction in space surveillance radars through an adaptive beamforming approach. Aerospace, 11(6). URL: https://www.mdpi.com/2226-4310/11/6/451. doi:10.3390/aerospace11060451.
Montaruli, M.F., De Luca, M.A., Massari, M., et al., 2024c. Operational angular track reconstruction in space surveillance radars through an adaptive beamforming approach. Aerospace 11 (6), 451.
Montaruli, M.F., Di Lizia, P., Cordelli, E., et al., 2023b. A stochastic approach to detect fragmentation epoch from a single fragment orbit determination. Adv. Space Res. 72 (9), 3713–3733. https://doi.org/10.1016/j.asr.2023.08.031.
Montaruli, M.F., Di Lizia, P., Tebaldini, S., et al., 2024d. Delta-k approach for space surveillance multireceiver radars. Astrodynamics. https://doi.org/10.1007/s42064-024-0217-5.
Montaruli, M.F., Facchini, L., Faraco, N., et al., 2025. Third long-march 5b re-entry campaign through italian space surveillance radars. Adv. Space Res. 75 (2), 2139–2155.
Montaruli, M.F., Lizia, P.D., Cordelli, E., et al., 2023c. A stochastic approach to detect fragmentation epoch from a single fragment orbit determination. Adv. Space Res. https://doi.org/10.1016/j.asr.2023.08.031, URL: https://www.sciencedirect.com/science/article/pii/S0273117723006798.
Montaruli, M.F., Purpura, G., Cipollone, R., et al., 2024e. An orbit determination software suite for space surveillance and tracking applications. CEAS Space Journal. https://doi.org/10.1007/s12567-024-00535-1.
Montaruli, M.F., Purpura, G., Cipollone, R. et al., 2022. A software suite for orbit determination in space surveillance and tracking applications. In: 9th European Conference for Aerospace Sciences (EUCASS 2022) (pp. 1–12).
Muciaccia, A., Facchini, L., Montaruli, M.F., et al., 2023. Radar observation and recontruction of cosmos 1408 fragmentation. J. Space Safety Eng. https://doi.org/10.1016/j.jsse.2023.11.006, URL: https://www.sciencedirect.com/science/article/pii/S2468896723001131.
Muciaccia, A., Romano, M., Trisolini, M., et al., 2024. Reconstruction of in-orbit breakup events over the long term. Acta Astronaut.
NASA-JPL (Accessed: 2023). The spice toolkit.https://naif.jpl.nasa.gov/-naif/toolkit.html.
Osweiler, V.P., 2006. Covariance Estimation and Autocorrelation of NORAD Two-Line Element Sets. Master's thesis Air Force Institute of Technology Wright-Patterson Air Force Base, Ohio. URL: https://scholar.afit.edu/etd/3531 advisor: Nathan A. Titus, PhD. DTIC Accession Number: ADA446817.
Pardini, C., Anselmo, L., 2008. Impact of the time span selected to calibrate the ballistic parameter on spacecraft re-entry predictions. Adv. Space Res., 41(7), 1100–1114. URL: https://www.sciencedirect.-com/science/article/pii/S0273117707010988. doi: 10.1016/j.asr.2007.11.013.
Pardini, C., Anselmo, L., 2023. The short-term effects of the cosmos 1408 fragmentation on neighboring inhabited space stations and large constellations. Acta Astronaut. 210, 465–473. https://doi.org/10.1016/j.actaastro.2023.02.043.
Pastor, A., Escribano, G., Sanjurjo-Rivo, M., et al., 2022. Satellite maneuver detection and estimation with optical survey observations. J. Astronaut. Sci. 69 (3), 879–917. https://doi.org/10.1007/s40295-022-00311-5, URL: https://www.scopus.com/inward/record.uri?eid=2-s2.0-85131520993&doi=10.1007%2fs40295-022-00311-5&partnerID=40&md5=c3cc1c7a6ef0c5cecc1f7734328dc9d3.
Siminski, J., 2016. Techniques for assessing space object cataloguing performance during design of surveillance systems. In: In 6th International Conference on Astrodynamics Tools and Techniques (ICATT), pp. 14–17.
Slatton, Z., McKissock, D., 2017. Methods of predicting and processing breakups of space objects. In Proceedings of the 7th European Conference on Space Debris. Darmstadt, Germany: European Space Agency/ ESA Space Debris Office. URL: https://conference.sdo.esoc.esa.int/proceedings/sdc7/paper/208/SDC7-paper208.pdf presented at ESA/ESOC, Darmstadt, Germany, 18–21 April 2017.
Space-Track (Accessed: 2023). Space-track website. https://www.space-track.org/auth/login 18th Space Defense Squadron.
Vallado, D., Crawford, P., Hujsak, R. et al., 2006. Revisiting spacetrack report# 3. In: AIAA/AAS astrodynamics specialist conference and exhibit (p. 6753).
Vittaldev, V., Russell, R.P., Linares, R., 2016. Spacecraft uncertainty propagation using gaussian mixture models and polynomial chaos expansions. J. Guid., Control, Dynam. 39 (12), 2615–2626.
Vittaldev, V. et al., 2015. Uncertainty propagation and conjunction assessment for resident space objects Ph.D. thesis.